53-43 Ma Deformation of Eastern Tibet Revealed by Three Stages of Tectonic Rotation in the Gongjue Basin

Yang Zhang, Wentao Huang, Baochun Huang, Douwe J.J. van Hinsbergen, Yang Tao, Guillaume Dupont-Nivet, Zhaojie Guo

Journal of Geophysical Research: Solid Earth

RESEARCH ARTICLE
10.1002/2018JB015443

Key Points:
- The maximum deposition age of the Gongjue red beds is of 52.5 ± 1.5 Ma
- Primary remanence carried by detrital magnetite and hematite can be isolated
- A net CW rotation of 24.1° occurred with three stages recognized: 33.3° CW and 26.9° CCW during 53–43 Ma, and 17.7° CW rotations after 43 Ma

Supporting Information:
- Supporting Information S1

Correspondence to:
W. Huang and Z. Guo,
whuang28@ur.rochester.edu;
zjguo@puk.edu.cn

Citation:
Zhang, Y., Huang, W., Huang, B., van Hinsbergen, D. J. J., Yang, T., Dupont-Nivet, G., & Guo, Z. (2018). 53–43 Ma deformation of eastern Tibet revealed by three stages of tectonic rotation in the Gongjue basin. *Journal of Geophysical Research: Solid Earth*, *123*. https://doi.org/10.1002/2018JB015443

Received 6 JAN 2018
Accepted 26 MAR 2018
Accepted article online 30 MAR 2018

53–43 Ma Deformation of Eastern Tibet Revealed by Three Stages of Tectonic Rotation in the Gongjue Basin

Yang Zhang[1], Wentao Huang[2,3,4], Baochun Huang[1], Douwe J. J. van Hinsbergen[5], Tao Yang[6], Guillaume Dupont-Nivet[1,7,8], and Zhaojie Guo[1]

[1]Key Laboratory of Orogenic Belts and Crustal Evolution, Ministry of Education, School of Earth and Space Sciences, Peking University, Beijing, China, [2]Department of Geosciences, University of Arizona, Tucson, AZ, USA, [3]Department of Geology and Geophysics, University of Utah, Salt Lake City, UT, USA, [4]Department of Earth and Environmental Sciences, University of Rochester, Rochester, NY, USA, [5]Department of Earth Sciences, Utrecht University, Utrecht, The Netherlands, [6]Hubei Subsurface Multi-Scale Imaging Key Laboratory, Institute of Geophysics and Geomatics, China University of Geosciences, Wuhan, China, [7]Géosciences Rennes, UMR 6118, Université de Rennes 1, Campus de Beaulieu, Rennes, France, [8]Institute of Earth and Environmental Science, University of Potsdam, Potsdam, Golm, Germany

Abstract The Gongjue basin from the eastern Qiangtang terrane is located in the transition region where the regional structural lineation curves from east-west-oriented in Tibet to north-south-oriented in Yunnan. In this study, we sampled the red beds in the basin from the lower Gongjue to upper Ranmugou formations for the first time covering the entire stratigraphic profile. The stratigraphic ages are bracketed within 53–43 Ma by new detrital zircon U-Pb ages constraining the maximum deposition age to 52.5 ± 1.5 Ma. Rock magnetic and petrographic studies indicate that detrital magnetite and hematite are the magnetic carriers. Positive reversals and fold tests demonstrate that the characteristic remanent magnetization has a primary origin. The Gongjue and Ranmugou formations yield mean characteristic remanent magnetization directions of $D_s/I_s = 31.0°/21.3°$ and $D_s/I_s = 15.9°/22.0°$, respectively. The magnetic inclination of these characteristic remanent magnetizations is significantly shallowed compared to the expected inclination for the locality. However, the elongation/inclination correction method does not provide a meaningful correction, likely because of syn-depositional rotation. Rotations relative to the Eurasian apparent polar wander path occurred in three stages: Stage I, 33.3 ± 3.4° clockwise rotation during the deposition of the Gongjue and lower Ranmugou formations; Stage II, 26.9 ± 3.7° counterclockwise rotation during deposition of the lower and middle Ranmugou formation; and Stage III, 17.7 ± 3.3° clockwise rotation after 43 Ma. The complex rotation history recorded in the basin is possibly linked to sinistral shear along the Qiangtang block during India indentation into Asia and the early stage of the extrusion of the northwestern Indochina blocks away from eastern Tibet.

1. Introduction

Unraveling the kinematic history of the Cenozoic India-Asia collision and associated growth of the Himalayas and Tibetan Plateau is key to identify the underlying geodynamic forcing as well as the regional crustal response. Plate reconstruction demonstrates that 4,000–5,000 km of convergence (Copley et al., 2010; van Hinsbergen, Steinberger, et al., 2011) has occurred since the initiation of the collision at ~58 Ma (e.g., DeCelles et al., 2014; Hu, Garzanti, et al., 2015; Ormeet al., 2014), up to 1,000–1,200 km of which must have been partitioned into Asian lithospheric crustal shortening and extrusion (Chen et al., 1993; Cheng et al., 2015; Johnson, 2002; Replumaz & Tapponnier, 2003; van Hinsbergen, Kapp, et al., 2011). Aside from the N-S shortening in Tibet, a significant component of convergence was in eastern Tibet accommodated by the extrusion of the Indochina terrane along the Ailao Shan fault over a distance of ~600 km, as revealed by geological and paleomagnetic studies (e.g., Li, Advokaat, et al., 2017; Royden et al., 2008; Tapponnier et al., 1982; Yang & Besse, 1993). In the past few decades, paleomagnetic data have been widely used to constrain paleolatitude and vertical axis rotations of these intensely deformed Asian terranes to aid the reconstruction of the post-collisional crustal shortening and extrusion (e.g., Chen et al., 1993, 2010, 2014; Cogné et al., 1999; Ding et al., 2015; Dupont-Nivet, Lippert, et al., 2010; Huang et al., 1992, 2013; Huang, Dupont-Nivet, Lippert, van Hinsbergen, Dekkers, Waldrip, et al., 2015; Huang, van Hinsbergen, et al., 2015; Huang & Opdyke, 2015; Li, Yang, et al., 2017; Li et al., 2018; Lippert et al., 2011; Ma et al., 2014, 2017; Tong, Yang, Wang, et al., 2015; Tong et al., 2016; van Hinsbergen et al., 2012; Yan et al., 2017; Yang et al., 2015; Yi et al., 2011; Zhao et al., 2015). However, paleomagnetic investigations of the Lhasa and Qiangtang terranes are mostly from the western and middle parts of Tibet, whereas few data are available from the eastern part, where the

Qiangtang-Sibumasu terrane curves around the eastern Himalayan syntaxis and where the extruded Indochina-related blocks originated (e.g., Li, Advokaat, et al., 2017).

Studying the rotation history of the Qiangtang terrane in eastern Tibet is of particular importance because it has direct implications on the existence, the timing, and the magnitude of tectonic processes that have been proposed to accommodate the Indian indentation, crustal shortening (Lippert et al., 2011), lateral extrusion (Tapponnier et al., 1982), or dextral shear and oroclinal bending (England & Molnar, 1990). The intriguing arcuate shape of the eastern end of the Lhasa and Qiangtang terranes strongly suggests that it has been acquired through clockwise rotations in response to the northward indentation of India into Asia and relative to the rigid South China block to the east (Chen & Gerya, 2016; Dupont-Nivet et al., 2004). The proposed mechanisms indicate that variations of lateral crustal strength during the India-Asia collision and the development of an orogenic plateau implied significant crustal rotations in response to lithospheric processes such as lower crustal flow or roll back of the oceanic slab adjacent to the collision (e.g., Cook & Royden, 2008; Pusok & Kaus, 2015). Moreover, the extrusion inevitably leads to rotations of the crustal units in the south of the extruding domain, counterclockwise in the west and clockwise in the east. Identifying the units that underwent major rotations and their timing may thus help to determine from where and when oroclinal bending and extrusion occurred, both of which are greatly debated due to direct implication on models of the collision.

By comparing Tibetan structures with those of an analogue sandbox model (Tapponnier et al., 1982), a hypothesis was put forward that Indochina has been extruded from between the Lhasa and Qiangtang terranes (e.g., Replumaz & Tapponnier, 2003; Royden et al., 2008). However, Indochina is located to the northeast of the Sibumasu terrane, and Sibumasu is widely considered to have paleogeographically been contiguous with the Qiangtang terrane, similar to today (e.g., Metcalfe, 2013; Pubellier et al., 2008). Restoring Indochina along the Bangong-Nujiang suture would require breaking the Qiangtang-Sibumasu terrane into two. Li, Advokaat, et al. (2017) therefore rather suggested that northwestern Indochina blocks were located to the northeast and north of the Qiangtang-Sibumasu terrane and extruded along the Jinsha suture instead. The paleomagnetic constraints on northeastern Indochina blocks suggested that extrusion started in Eocene times and was accommodated by internal shortening and block rotation in NW Indochina, followed by an Oligocene-Early Miocene phase of extrusion along the entire Ailao Shan-Red River fault (Li, Advokaat, et al., 2017). Testing whether the eastern Qiangtang terrane was involved in the oroclinal bending associated with this extrusion may provide a test for these scenarios.

The Cenozoic Gongjue basin, which lies in the transition region where east-west-oriented geological trends in the west are gradually deflected into north-south trends in the south and east, is therefore more suitable for revealing the evolutionary relationships of the central and eastern Tibetan Plateau and the extruded Indochina block during the India-Asia collision. A recent paleomagnetic study of the Eocene red beds in the Gongjue basin suggested that the basin experienced ~24° of clockwise rotation with respect to Eurasia at some undefined time after sediment deposition (Tong et al., 2017). However, the study covered only a small part of the basin stratigraphy such that it remains unclear whether the rotation occurred during or after filling of the basin.

In this paper, we reevaluate the geochronology and paleomagnetically analyze the complete stratigraphic section of the red beds in the Gongjue basin to attempt placing time constraints on the rotation estimated by Tong et al. (2017). The following approaches were used: (1) Detrital zircon U-Pb geochronologic dating was applied on the Gongjue red beds to constrain the deposition age. (2) Large number of samples for paleomagnetic investigations in two sections in the middle and southern parts of the basin covering the entire stratigraphic profile was collected. (3) Comprehensive rock magnetic experiments, including thermomagnetic experiments, hysteresis loops, isothermal remanent magnetization (IRM) and back-field acquisition, and anisotropy of magnetic susceptibility (AMS) measurements, were provided to identify magnetic carriers and fabrics. (4) Scanning electron microscopy (SEM) observation and energy-dispersive X-ray spectrometry (EDS) analysis were used to define the origin of the magnetic minerals via morphology and verify rock magnetic results. (5) Thermal demagnetization was used to isolate paleomagnetic directions from the red beds in the Gongjue basin. (6) Reversals and fold tests were applied to estimate when the remanence was acquired. (7) Finally, the variation of the declination along the stratigraphic profile was analyzed. With this information, the origin and age of the remanence isolated from the Gongjue red beds are evaluated. Finally, the results are placed in context of kinematic restoration of eastern Tibet in connection to the extrusion of the Indochina-related blocks.

2. Geological Background and Sampling

The Qiangtang terrane is one of the major Gondwana-derived units that make up the crust of central Tibet (Figure 1a). It sits between the Songpan-Ganzi and Lhasa terranes with the Latest Triassic Jinsha suture to the north and the Late Jurassic-Early Cretaceous Bangong-Nujiang suture to the south (e.g., Kapp et al., 2007; Sensor & Natalin, 1996; Yin & Harrison, 2000; Zhu et al., 2011; Yang et al., 2012). It is approximately east-west-trending in the west and central parts with a maximum width of 400–500 km but narrows to $<$150 km in the eastern part and gradually deflects into a north-south orientation in the region north and east of the eastern Himalayan syntaxis. There it is contiguous with the Sibumasu terrane that forms the main units of Sundaland (Metcalfe, 2013). During the early stage of the India-Asia collision, deformation along these and other suture zones resulted in substantial Cenozoic shortening and strike-slip faulting (Kapp et al., 2005) and a series of small thrust related basins developed along the northern part of the Qiangtang terrane (Horton et al., 2002).

The long (~200 km) and narrow Gongjue basin is one of these fault-bounded Cenozoic basins situated in the eastern part of the Qiangtang terrane and directly north of the eastern Himalayan syntaxis (Figure 1b). The structure of the Gongjue basin is characterized by reverse faults and a basin-scale asymmetrical syncline with a much thicker western than eastern limb suggesting syn-sedimentary west-verging deformation (Figures 1c and 1d). To the east, the basin is in fault contact with or unconformably overlies Carboniferous to Triassic strata of the Qiangtang terrane. To the west, Triassic strata cut and thrust upon the basin sediments. Small-scale folds also developed in the upper part of the stratigraphy near the core of the syncline. The fold axes are nearly horizontal and parallel to the strike of the bedding, and the overall orientation of the basin (Figure 1b). The basin fill is dominated by Eocene red clastic sediments (sandstone, siltstone, and conglomerate) and evaporites (carbonates, gypsum, and salt), interpreted to have predominantly been deposited in an alluvial fan, fan-delta, floodplain, and lacustrine environment (Studnicki-Gizbert et al., 2008). The stratigraphy is subdivided into the Gongjue formation (E_{2g}) and the Ranmugou formation (E_{2r}; Bureau of Geology and Mineral Resources of Xizang Autonomous Region, 1993). The Ranmugou formation overlies the Gongjue formation conformably and consists of a lower part (E_{2r}^1), a middle part (E_{2r}^2), and an upper part (E_{2r}^3; Figures 1c and 1d). Volcanic rocks with eruption age of ~44–43 Ma dated by feldspar and biotite phenocrysts $^{40}Ar/^{39}Ar$ and zircon U-Pb methods are well exposed in E_{2r}^2 in the northern part of the basin (Studnicki-Gizbert et al., 2008; Tang et al., 2017).

The stratigraphy of the Gongjue basin is particularly well exposed in the southern and middle parts of the basin, where the total thickness is up to 5 km. Tong et al. (2017) sampled several paleomagnetic sites in the upper Gongjue formation and lower Ranmugou formation. We complement here that data set by the collection of 63 sites (623 individual paleomagnetic cores, 8–13 cores from each site) covering the entire E_{2g} and E_{2r} in two sections. A total of 29 sites (315 cores) were collected from E_{2g} (GJ1–GJ24) and E_{2r}^1 (GJ25–GJ29) in the AA′ section in the southern part of the basin, and 34 sites (308 cores) were collected from E_{2g} (JD1–JD5), E_{2r}^1 (JD6–JD7), E_{2r}^2 (JD8–JD23), and E_{2r}^3 (JD24–JD34) in the BB′ section in the middle part of the basin (Figures 1c and 1d). Drilled paleomagnetic cores were oriented with both magnetic and sun compasses. Besides, we also collected six block samples at the paleomagnetic sampling localities (GJ7, GJ20, and GJ24 in the AA′ section and JD8, JD14, and JD21 in the BB′ section; Figures 1c and 1d) for detrital zircon U-Pb geochronologic analysis.

3. Geochronology

Detrital zircon U-Pb geochronologic analysis was conducted at the Key Laboratory of Orogenic Belts and Crustal Evolution, Peking University, using a laser ablation-inductively coupled plasma-mass spectrometer. Methods and procedures for U-Pb zircon geochronology are the same as the geochronologic analysis presented in Huang, van Hinsbergen, et al. (2015). In this study, we aim at calculating the best age for the youngest population of zircon to constrain the maximum depositional age of the Gongjue red beds. Of the 527 individual detrital zircon grains dated from these six samples, a population of 16 zircon grains from three samples (GJ24, JD8, and JD21) has yielded concordant ages of 47.7 to 59.3 Ma (Figure 2a; Table S1 in the supporting information). The weighted mean $^{206}Pb/^{238}U$ age of these younger grains is of 52.5 ± 1.5 Ma (mean square weighted deviation = 12; Figure 2b). We use this weighted mean age to estimate the maximum depositional age of the Gongjue red beds. Together with the recent feldspar and biotite $^{40}Ar/^{39}Ar$ and zircon U-Pb

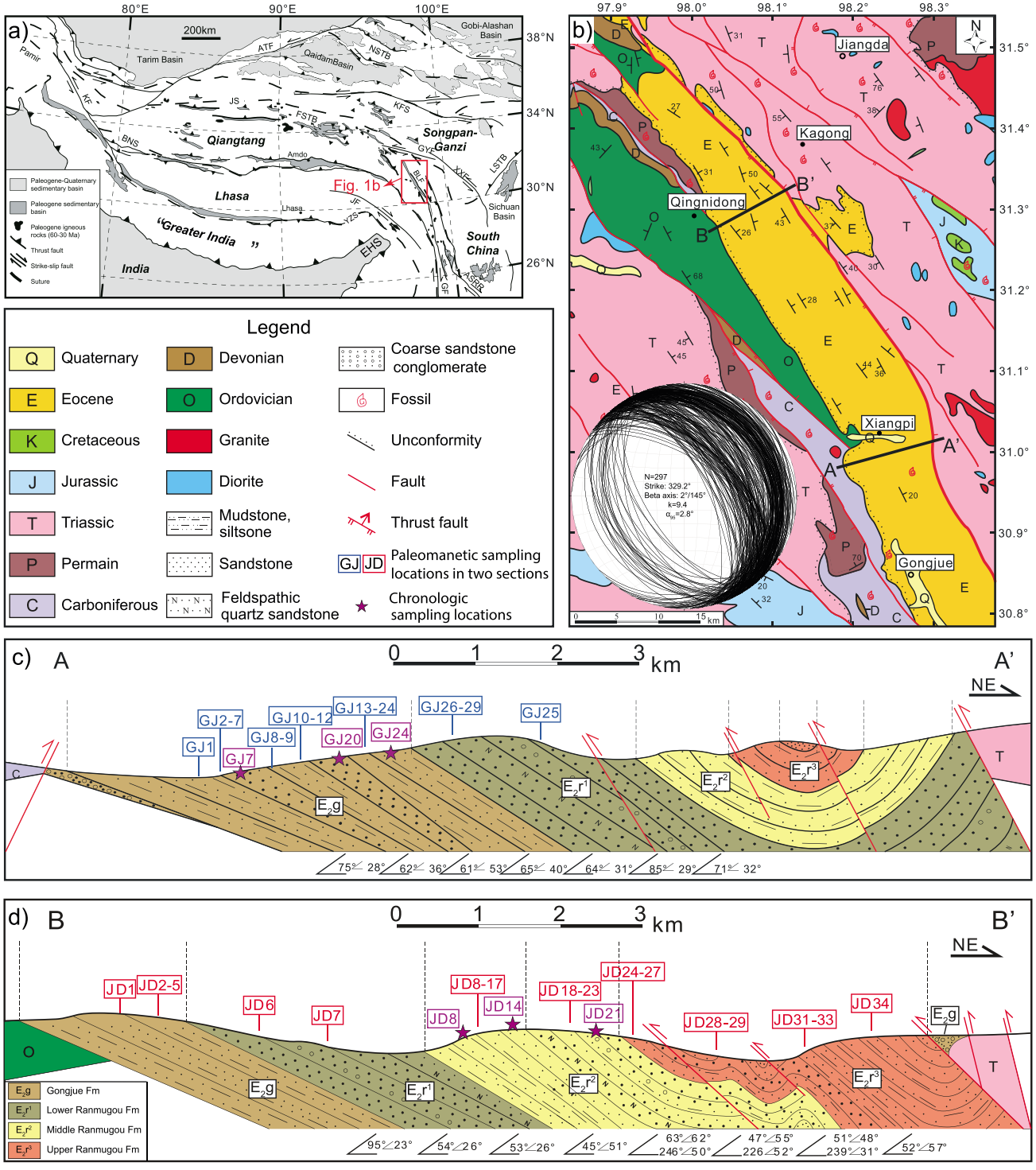

Figure 1. (a) Simplified tectonic map of the Tibetan Plateau, modified from Spurlin et al. (2005). ASRR, Ailao Shan-Red River fault; JS, Jinsha suture; BNS, Banggong-Nujiang suture; YZS, Yarlung Zangbo suture; EHS eastern Himalayan syntaxis; other abbreviations are the same as Spurlin et al. (2005). (b) Geological map of the Gongjue basin and surrounding area. (c, d) Profile of the two sampled sections in the middle and southern part of the basin. E_{2g}, Gongjue formation; $E_{2r}^{1/2/3}$, lower/middle/upper of the Ranmugou formation.

dating of the volcanic rocks in E_2r^2 in the northern part of the Gongjue basin at 43.83 ± 0.27 Ma (feldspar and biotite $^{40}Ar/^{39}Ar$) and 43.2 ± 0.2 Ma (zircon U-Pb; Studnicki-Gizbert et al., 2008; Tang et al., 2017), the Gongjue formation and lower and middle Ranmugou formations were probably deposited within ca. 53 to 43 Ma.

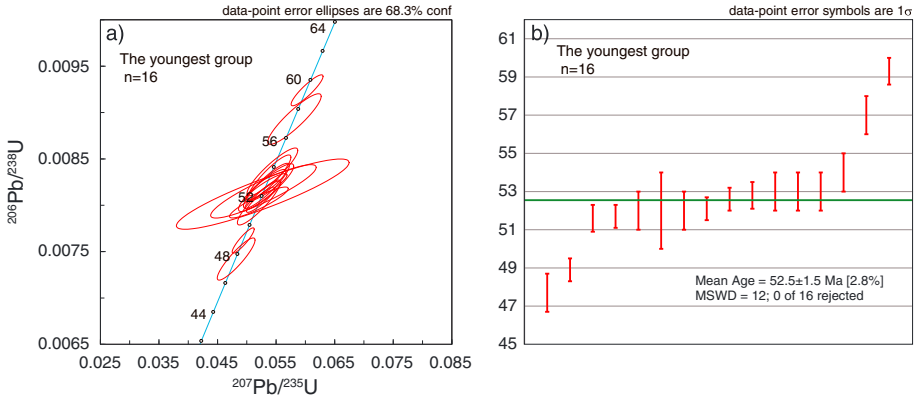

Figure 2. Concordia plots (a) and mean average (b) of the U-Pb dating of the 16 youngest detrital zircons from three samples (GJ24, JD8, and JD21). MSWD, mean square weighted deviation.

4. Rock Magnetism

Rock magnetic analyses were conducted at Utah Paleomagnetic Center at the University of Utah (USA) and Institute of Geophysics, China Earthquake Administration (Beijing).

4.1. Thermomagnetic Experiments

High-temperature, low-field susceptibility experiments were performed in air on seven powdered specimens (20–30 mg) using a KLY-2 Kappabridge AC susceptibility meter with an AC field of 300 A m^{-1} and a frequency of 920 Hz equipped with a CS2 heating device (AGICO, Brno, Czech Republic). Stepwise thermomagnetic runs with maximum temperatures of 300, 500, 600, and 700 °C were applied with intermittent cooling to room temperature. Susceptibility of the Gongjue red beds shows a progressive, quasi-reversible decrease up to 700 °C during heating (Figures 3a–3c). In general, two magnetic phases can be recognized based on the observed sharp decreases up to 580 and 680 °C in susceptibility slope of the thermomagnetic runs (Figures 3a–3c). Each magnetic phase contributes differently to the susceptibility from sample to sample. We interpret these magnetic behaviors to indicate the presence of magnetite and hematite as the magnetic carriers (Dunlop & Ödemir, 1997).

4.2. Hysteresis Loops, IRM and back-Field Curves, and IRM Component Analysis

Magnetic hysteresis loops, IRM acquisition, and back-field curves for 24 specimens (mass of 0.3–0.5 g; 12 from each of the two sections) were measured to determine hysteresis parameters, coercive force (B_c), remanence coercivity (B_{cr}), saturation remanence (M_r), and saturation magnetization (M_s) with a MicroMag™ Model 3900 vibrating sample magnetometer (Princeton Measurements Corp.) with a sensitivity of 5×10^{-10} A m^2. The maximum applied field was 1 T.

Hysteresis loops of the Gongjue red beds are all wasp waisted (Figures 3d–3f), indicating the existence of more than one magnetic phases with strongly contrasting coercivities (Roberts et al., 1995; Tauxe et al., 1996). IRM acquisition curves of the corresponding specimens remain unsaturated up to 1 T (Figures 3g–3i), reflecting the presence of high coercivity minerals, such as hematite. The B_c and B_{cr} values are ~26–190 and ~75–268 mT, respectively (Table S3 in the supporting information).

To quantitatively estimate the contributions of different magnetic minerals, we applied IRM component analysis to 11 specimens (Kruiver et al., 2001a). Three IRM components are used to fit the IRM acquisition curves: component 1 with $B_{1/2}$ (the field when half of saturation IRM (SIRM) is acquired) of ~10 mT and dispersion parameter (DP) of ~0.45 (log units); a relatively harder component 2 with $B_{1/2}$ of 20–100 mT and DP of 0.30–0.40; and a much harder component 3 with highest $B_{1/2}$ of ~400 mT and notably similar DP of ~0.20 (Figures 3j–3l; Table S4 in the supporting information). Component 1 contributes ~5% to the SIRM and might be the result of thermally activated component 2 (Egli, 2004; Heslop et al., 2004). Component 2 can be interpreted to be magnetite (Kruiver et al., 2001a). It contributes ~25–30% to the SIRM and is a subordinate magnetic carrier in the Gongjue red beds. Component 3 is the predominant

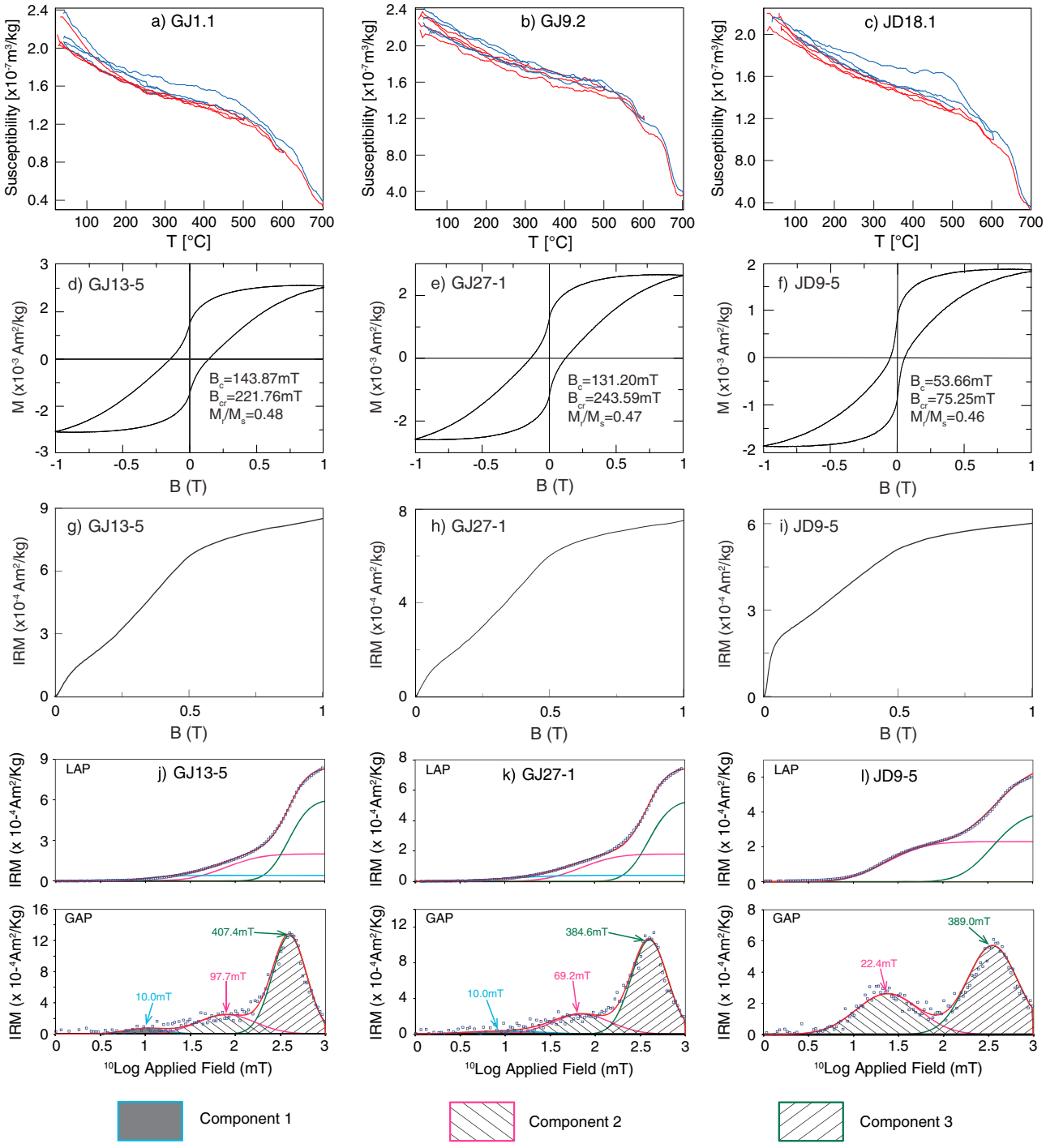

Figure 3. (a–c) Stepwise heating (red) and cooling curves (blue) of magnetic susceptibility in air for representative specimens. (d–i) Hysteresis loops and IRM acquisition curves for characteristic samples. (j–l) Isothermal remanent magnetization component analysis results of typical specimens with 150 data points acquired (Kruiver et al., 2001a). M, magnetization; B, magnetic induction; LAP, linear acquisition plot; GAP, gradient acquisition plot.

magnetic carrier in the Gongjue red beds and contributes ~60–70% to the SIRM. It is not saturated up to 1 T and represents hematite (Kruiver & Passier, 2001).

In summary, thermomagnetic and hysteresis experiments consistently indicate that magnetic carriers of the Gongjue red beds are dominated by hematite and magnetite, which also record the magnetic fabric.

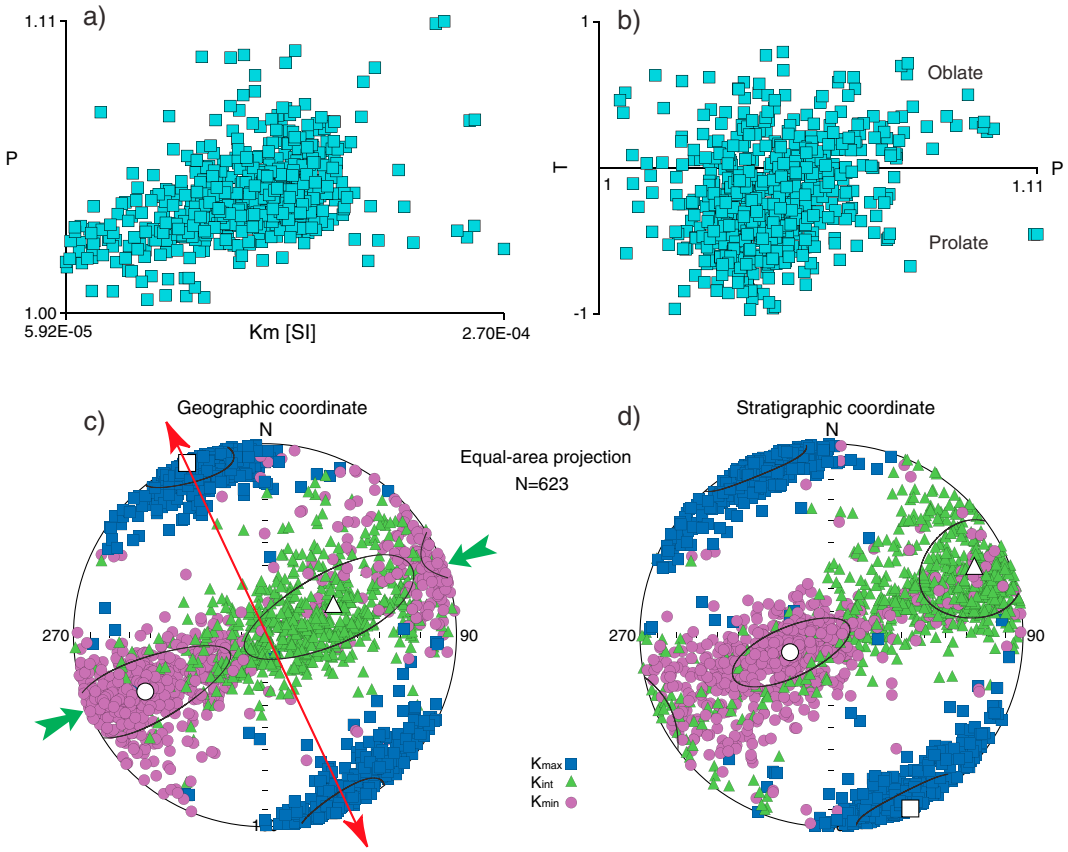

Figure 4. Magnetic fabric studies of the red beds in the Gognjue basin based on AMS measurements. (a) Magnetic susceptibility (Km) versus anisotropy (*P*) plot. (b) Anisotropy (*P*) versus shape parameter (*T*) plot. (c, d) Stereoplots of the AMS results in geographic (c) and stratigraphic (d) coordinates. Solid symbols, individual directions; open symbols, mean directions with 95% confidence limit. The green and red arrows represent the inferred compression and extension directions, respectively.

4.3. AMS

We determined the composite fabric of the magnetic grains by measuring the AMS of 623 sedimentary samples (315 from the AA′ section and 308 from the BB′ section) with a MFK1-FA Multi-Function Kappabridge susceptometer, in an applied field of 200 A/m with a frequency of 976 Hz. Several parameters are used to characterize the observed magnetic fabric: the degree of anisotropy, P (K_{max}/K_{min}); magnetic lineation, L (K_{max}/K_{int}); magnetic foliation, F (K_{int}/K_{min}); and the shape parameter, T ($T = (\ln F - \ln L)/(\ln F + \ln L)$), where K_{max}, K_{int}, and K_{min} are the principal axes of the calculated triaxial ellipsoids from the AMS measurements (Jelinek, 1981).

The AMS results of the AA′ section are indistinguishable from those of the BB′ section, and we therefore combine the two sections for description below. Magnetic susceptibility of the Gongjue red beds are between 5.92×10^{-5} and 2.70×10^{-4} SI (Figure 4a; Table S2 in the supporting information). P varies from 1.005 to 1.110, with an average of 1.044 (Figure 4a; Table S2 in the supporting information). AMS measurement shows a magnetic fabric dominated by prolate ellipsoids, although both prolate and oblate ellipsoids are observed (Figure 4b).

The in situ K_{max} axes of AMS show a NWN-SES orientation, which is similar to the regional strike (~330°) of the Gongjue basin (Figure 1c) and thus suggests ENE-WSW tectonic contraction. After tilt correction, the mean K_{min} axes are broadly distributed in a girdle, and their mean is not perpendicular to the bedding but is deflected approximately ~19° southwestward from the pole of the bedding planes (Figure 4d). This indicates that the original sedimentary fabric have been affected by the compression as recognized in both experimental and theoretical studies (Hrouda, 1991; Jezek & Gilder, 2006).

5. SEM Observation and EDS Analysis

To investigate the morphology of the magnetic minerals that may help evaluate their origin, we analyzed six thin sections of the Gongjue red beds (three from each of the two sections) with a Field Electron and Ion GEG-650 SEM, operated at 15 kV and 40–60 nA at the SEM lab at the Key Laboratory of Orogenic Belts and Crustal Evolution, School of Earth and Space Sciences, Peking University. EDS analysis was subsequently conducted to obtain compositional information.

Two types of detrital iron oxides are generally present in the thin sections. We interpret them to be magnetite and hematite based on their contrasting morphologic characteristics (Figure 5), the EDS analysis (Figure S1 in the supporting information), and the rock magnetic results in section 4. The size of the detrital magnetite grains varies widely from <10 to >200 μm (Figures 5a–5f, 5i, 5l, 5n, 5q–5s, and 5u–5w). Solid-state oxidation-exsolution characterized by distribution of Ti-rich ilmenite in the Ti-poor magnetite can be observed in most of the detrital magnetite grains (Figures 5b, 5d, 5f, 5i, 5n, 5q–5s, and 5u–5w; Figure S1 in the supporting information). Rutile and silicate mineral inclusions are also common in magnetite grains (Figure 5c). These features indicate a magmatic origin of the detrital magnetite within the Gongjue red beds (e.g., Turner et al., 2008). Some magnetite grains have been altered with voids formed within the crystals (Figures 5d, 5f, and 5i) or fine-grained authigenic hematite produced (Figure 5e). Detrital hematite grains range from <10 to up to 100 μm in size (Figures 5g, 5h, 5j, 5k, 5m, 5o, 5p, 5t, and 5x). They lack oxidation-exsolution features and usually have little Ti and Cr within the lattice (Figure S1 in the supporting information). Besides detrital iron oxides, another phase of iron oxide is fine-grained authigenic hematite. They were probably deposited during diagenetic mobility of iron from detrital magnetite (Figures 5e and 5w), hematite (Figures 5o and 5p), and iron-bearing silicate minerals (Figure 5v). This population of hematite is occasionally visible and is usually distributed around edges or fractures of detrital minerals.

These observations suggest that the predominant magnetic minerals within the Gongjue red beds, magnetite and hematite, have a primary detrital origin, whereas authigenic hematite has a very low abundance. Mineralogically, we conclude that the Gongjue red beds contain large amounts of detrital magnetite and hematite and show insignificant signs of alteration of detrital iron oxides and of formation of authigenic hematite.

6. Paleomagnetism

We isolated characteristic remanent magnetization (ChRM) directions of all the samples by thermal demagnetization. Samples are heated and cooled in a magnetically shielded ASC oven (Model TD48-SC) that has a residual field less than 10 nT. The natural remanent magnetization (NRM) was measured on a 2G Enterprises DC SQUID rock magnetometer (noise level 3×10^{-12} A m^2) at the Magnetotectonics Laboratory, Peking University. Samples were thermally demagnetized in ~18 steps up to 685 °C with 100 °C intervals below 500 °C and 3–20 °C intervals above 500 °C. Remanence components were determined by principal component analysis (Kirschvink, 1980) on at least five successive demagnetization steps with the platform independent portal http://paleomagnetism.org (Koymans et al., 2016). Stepwise demagnetization behavior is shown by the Zijderveld diagram (Zijderveld, 1967). Fisher (1953) statistics were used to calculate the mean direction.

For the Gongjue red beds, a low temperature viscous component with random direction was removed below 300 °C (Figure 6). At higher demagnetization temperature, nearly half of the samples showed erratic demagnetization trajectories that are not interpretable (Figures 6d and 5i), while others displayed a stable intermediate to high-temperature component decaying linearly toward the origin up to 680 °C (Figures 6a–6c, 6e–6h, and 6j–6p). We interpreted 328 stable ChRM directions of both normal and reversed polarities from the sampled Gongjue red beds in the two sections using principal component analysis (Table S5 in the supporting information). For samples from the Gongjue formation (GJ1–GJ24 and JD1–JD5, Figures 1c and 1d), the mean directions of the ChRMs of normal and reversed polarities are $D_s = 27.7°$, $I_s = 20.2°$ ($n = 74$, $k = 17.4$, $a_{95} = 4.1°$) and $D_s = 214.2°$, $I_s = -22.4°$ ($n = 76$, $k = 17.7$, $a_{95} = 4$) after tilt correction ("s" stands for stratigraphic coordinates and "g" stands for geographic coordinates), respectively (Figure 7a). We then convert ChRMs of reversed polarity to their antipodal directions and calculate the mean ChRM direction of the red beds from the Gongjue formation, which is $D_s = 31.0°$, $I_s = 21.3°$ ($n = 150$, $k = 16.8$, $a_{95} = 2.9°$; Figure 7a). For samples

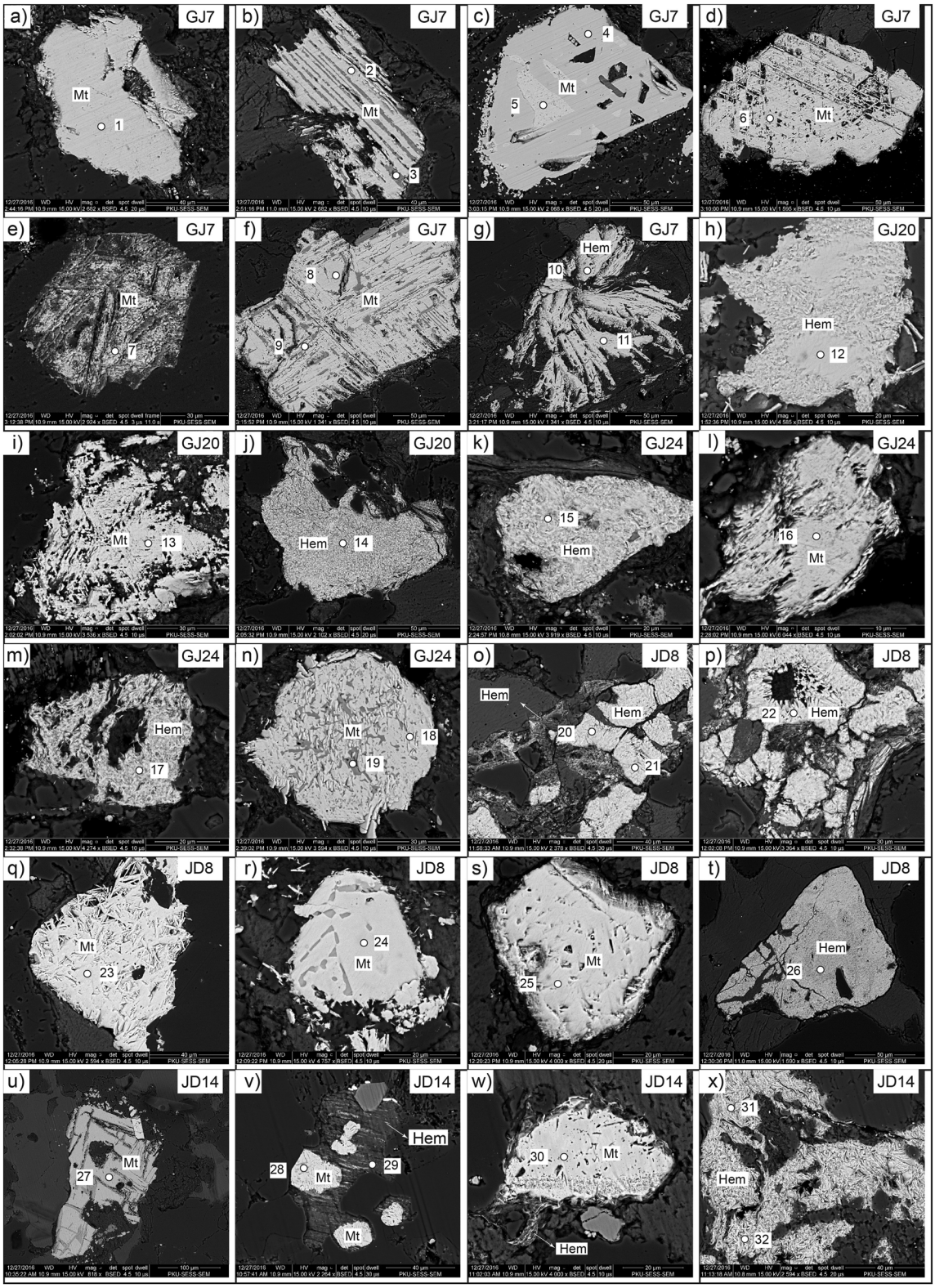

Figure 5. Scanning electron microscopy backscatter electron images for selected specimens from the red beds in the Gongjue Basin. Mt, magnetite; Hem, hematite. The white dots with numbers indicate EDS analysis spots as shown in Figure S1.

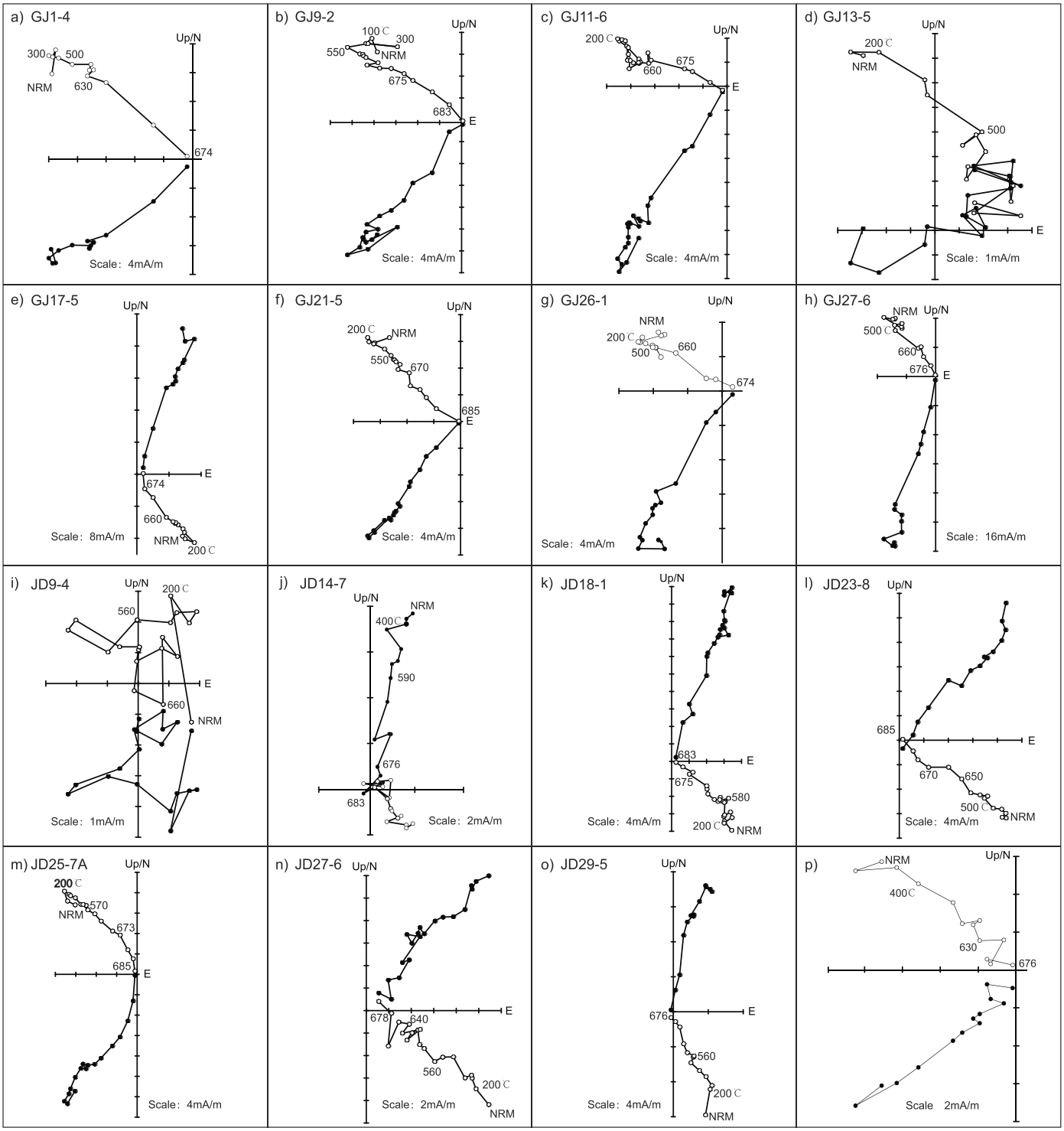

Figure 6. Representative demagnetization diagrams for specimens from the red beds in the Gongjue basin. All diagrams are displayed in stratigraphic coordinates. Closed (open) symbols represent declination (inclination).

from the Ranmugou formation (GJ25–GJ29 and JD6–JD34, Figures 1c and 1d), the mean directions of the ChRMs of normal and reversed polarities are D_s = 17.0°, I_s = 22.4° (n = 89, k = 14.9, a_{95} = 4.0°) and D_s = 194.8°, I_s = −21.5° (n = 89, k = 10.9, a_{95} = 4.8°) after tilt correction, respectively (Figure 7b). The mean ChRM direction of the red beds from the Ranmugou formation after converting ChRMs with reversed

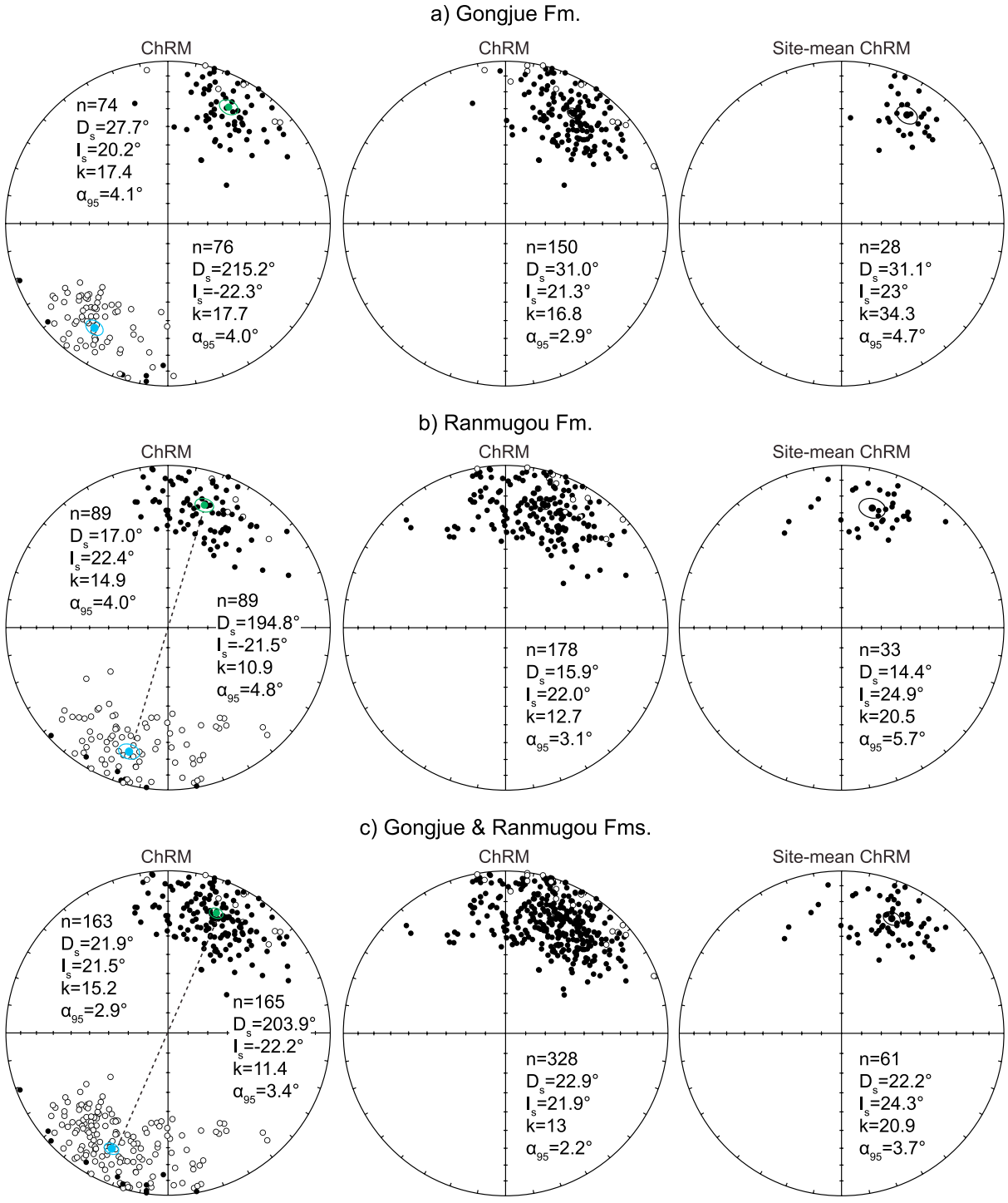

Figure 7. (a) Equal-area projections of individual ChRM directions (tilt corrected) from the Gongjue formation with both normal and reversed polarities (left), equal-area projections of ChRMs with reversed polarity transformed to antipodal directions (middle), and equal-area projections of site mean ChRMs with reversed polarity transformed to antipodal directions (right). (b) The same plots for individual ChRM directions from the Ranmugou formation (b) and combined two formations (c). Dots and circles represent mean ChRM directions and corresponding 95% confidence limit, respectively.

polarity to their antipodal directions is D_s = 15.9°, I_s = 22.0° (n = 178, k = 12.7, a_{95} = 3.1°; Figure 7b). We also combine results from both the Gongjue and Ranmugou formations and get the mean directions of the ChRMs of normal and reversed polarities, which are D_s = 21.9°, I_s = 21.5° (n = 163, k = 15.2, a_{95} = 2.9°) and D_s = 203.9°, I_s = −22.2° (n = 165, k = 11.4, a_{95} = 3.4) after tilt correction, respectively (Figure 7c). The mean

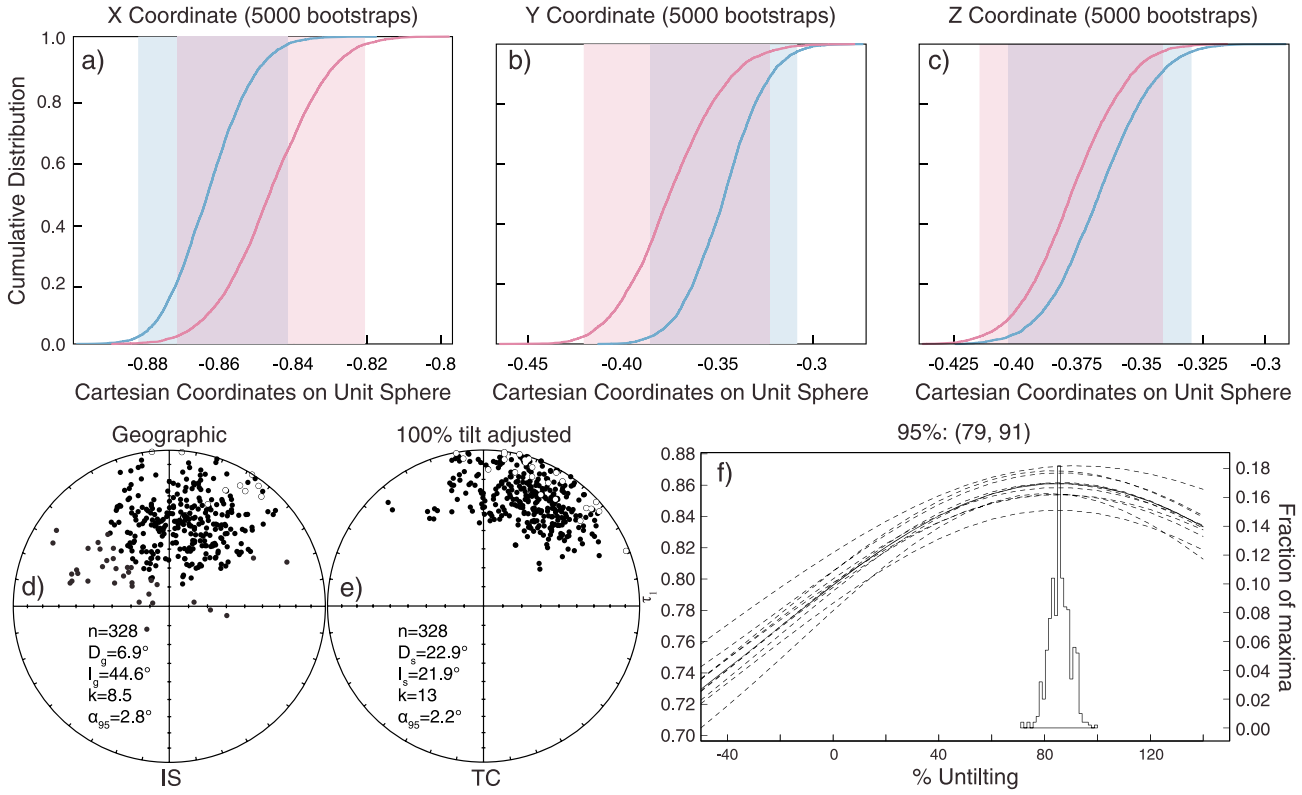

Figure 8. Nonparametric reversals test (a–c) and fold test (d–f) of ChRM directions isolated from the red beds from both Gongjue and Ranmugou formations in the Gongjue Basin (Tauxe, 2010; Tauxe & Watson, 1994).

ChRM direction of the Gongjue red beds after converting ChRMs with reversed polarity to their antipodal directions is D_s = 22.9°, I_s = 21.9° (n = 328, k = 13, a_{95} = 2.2°; Figure 7c). The average of the site mean ChRM directions is indistinguishable from the corresponding average of the individual ChRM directions (Figure 7; Tables S5 and S6 in the supporting information).

7. Discussion

7.1. Reliability of our Paleomagnetic Results

To constrain the origin of the remanence, we first apply the nonparametric reversals and fold tests (Tauxe, 2010; Tauxe & Watson, 1994). The nonparametric reversals test applied to the isolated ChRM directions of red beds from both the Gongjue formation and the Ranmugou formation shows that all three components of the bootstrapped coordinates for the normal and reversed sites overlap in confidence intervals (Figures 8a–8c), indicating that the normal and reversed ChRM directions are statistically indistinguishable and they share a common true mean direction at 95% confidence level. The reversals tests are thus positive. The nonparametric fold test applied to the ChRM directions from the Gongjue red beds is positive with a significant improvement of the k value from 8.5 to 13 after 100% tilt correction. The best grouping is at 79–91% untilting (Figures 8d–8f), suggesting a late syn-folding acquisition of the remanence; however, this is an artifact due to the syn-depositional rotation as described in our rotation analysis in section 7.2. Our rock magnetic tests, SEM observations, and EDS analysis further indicate that detrital magnetite and detrital hematite are the dominant magnetite carriers, whereas the diagenetic alteration of detrital magnetite and hematite and the formation of authigenic hematite are weak and rare (Figures 4 and 5). This is consistent with the absence of significant remagnetization presented above. Together, these observations show that the red beds in the Gongjue basin likely retain a primary depositional remanent magnetization, which is consistent with the previous argument of Tong et al. (2017).

We applied the elongation/inclination (E/I) correction to the ChRM directions from the Gongjue, Ranmugou formation, and combined formations separately to estimate the effect of the inclination shallowing, which is

common in clastic sedimentary rocks (e.g., Jackson et al., 1991; King, 1955; Kodama, 2009; Løvlie & Torsvik, 1984; Tauxe & Kent, 2004) and is widely recognized in Tibet and surrounding regions (e.g., Ding et al., 2015; Dupont-Nivet et al., 2002; Dupont-Nivet, van Hinsbergen, & Torsvik, 2010; Gilder et al., 2003; Huang et al., 2013; Huang, Dupont-Nivet, Lippert, Van Hinsbergen, Dekkers, Guo, et al., 2015; Li, Advokaat, et al., 2017; Tan et al., 2010; Yan et al., 2005). For the ChRM directions from the Gongjue formation, a flattening factor (*f*) of 0.65 [0.54, 0.81] is determined, and the mean inclination is corrected from 21.3 ± 4.3° to 29.9° with 95% confidence limits between 24.2° and 34.1° (Figure 9a). For the ChRM directions from the Ranmugou formation, a flattening factor (*f*) of 0.57 [0.49, 0.69] is determined, and the mean inclination is corrected to 33.3° with 95% confidence limits between 28.6° and 39° (Figure 9b). For the ChRM directions from both formations, a flattening factor (*f*) of 0.53 [0.48, 0.61] is determined, and the mean inclination is corrected from 21.6° to 34.2° [30.3°, 37.9°] (Figure 9c). These corrected inclinations would predict paleolatitudes of ~15–18°N for the Gongjue basin at ~53–43 Ma. These are unrealistic values as they are much lower than the predicted paleolatitude of the Qiangtang terrane of ~23–30°N constrained by robust paleomagnetic results of the Xialaxiu (51–49 Ma) and Nanqian (38–37 Ma; ~200 km northwestern of the Gongjue basin) volcanic rocks (Roperch et al., 2017) and the Wulanwulahu, Ejumaima, and Nading Co volcanic rocks (38–34 Ma) from the central Qiangtang terrane (Lippert et al., 2011). They are also inconsistent with the shallowing-corrected results of ~24°N by Tong et al. (2017) using the E/I and anisotropy-based methods. Therefore, the E/I method applied to our data set fails to give a meaningful correction for the inclination shallowing within the Gongjue red beds. The reasons for the failure will be discussed in section 7.2. We consider the inclinations as not representative of the paleolatitude. Nevertheless, inclination shallowing does not significantly affect the declination, and here we focus on rotation estimates derived from declination trends.

Compared to the paleomagnetic results of Tong et al. (2017), our results from the Gongjue formation, the Ranmugou formation, or the combined two formations are of systematic shallower inclinations and smaller declinations. Therefore, they are clearly different from the results of Tong et al. (2017). We attribute the differences mainly to the sampling strategy: our sampling covered both the Gongjue and Ranmugou formations of the entire stratigraphic profile, while Tong et al. (2017) mainly sampled along the strike of the bedding covering the upper part of the Gongjue formation and the lower part of the Ranmugou formation.

7.2. Stepwise Rotation of the Eastern Qiangtang Terrane

Careful inspection of the paleomagnetic data from the red beds in the Gongjue basin shows that the mean declination of the ChRMs from the Gongjue formation (31.0 ± 2.5°) is ~15° higher than that from the Ranmugou formation (15.9 ± 2.8°; Figures 7a and 7b), indicating that the red beds from the Gongjue formation and Ranmugou formation have experienced different rotational history. To reveal the rotational history of the basin recorded by the red beds, we analyzed the declinations of the ChRM directions. Site-mean ChRM directions were first calculated according to Fisher's statistics (Fisher, 1953). Sixty-one site-mean ChRM directions were determined in total (Table S6 in the supporting information), and the declinations of these site-mean ChRM directions were then plotted against the site level (the distance between adjacent sites was assigned to be "1"; Figure 10). The declinations of the site-mean ChRM directions vary upsection with a decreasing trend and then an increasing trend (Figure 10). To better characterize these trends, we applied a sliding window, averaging Fisher (1953) statistics for ChRM directions from 10 successive sites incrementally at each site. These moving averages of ChRM directions from 10 successive sites are likely averaging paleosecular variation. We then plotted the obtained window-mean declinations at site levels 5, 10, 15, 20, 25, 30, 35, 40, 45, 50, and 55 with respect to their site level (11 pairs in total) and compared to the expected declination determined from the Eurasian apparent polar wander path (APWP; Figure 10). A clockwise rotation and a following counterclockwise rotation are clearly indicated by progressive decrease and increase in declinations with the rotation change occurring between deposition of the E_{2r}^1 and E_{2r}^2. Significant linear correlations between declination and site level are observed in both clockwise and counterclockwise trends with the square of Pearson's correlation coefficients (R^2) between 0.8903 (lower) and 0.9366 (higher; Figure 10), respectively. These R^2 values are above the critical value of 0.833 for seven pairs and 0.934 for five pairs with $p = 0.02$. The window-mean declination at site level 55 is 25.7 ± 3.8°, indicating that the Gongjue basin has experienced a net clockwise rotation of 17.7 ± 3.3° with respect to the Eurasian APWP after the deposition of the Gongjue red beds (Torsvik et al., 2012). The window-mean declination at site level 35 is 0.8 ± 5.4°, which means the window-mean declination at this site level was −16.9 ± 4.5° soon after deposition of E_{2r}^3. This implies that the Gongjue basin was rotated 26.9 ± 3.7° counterclockwise relative to the Eurasian APWP

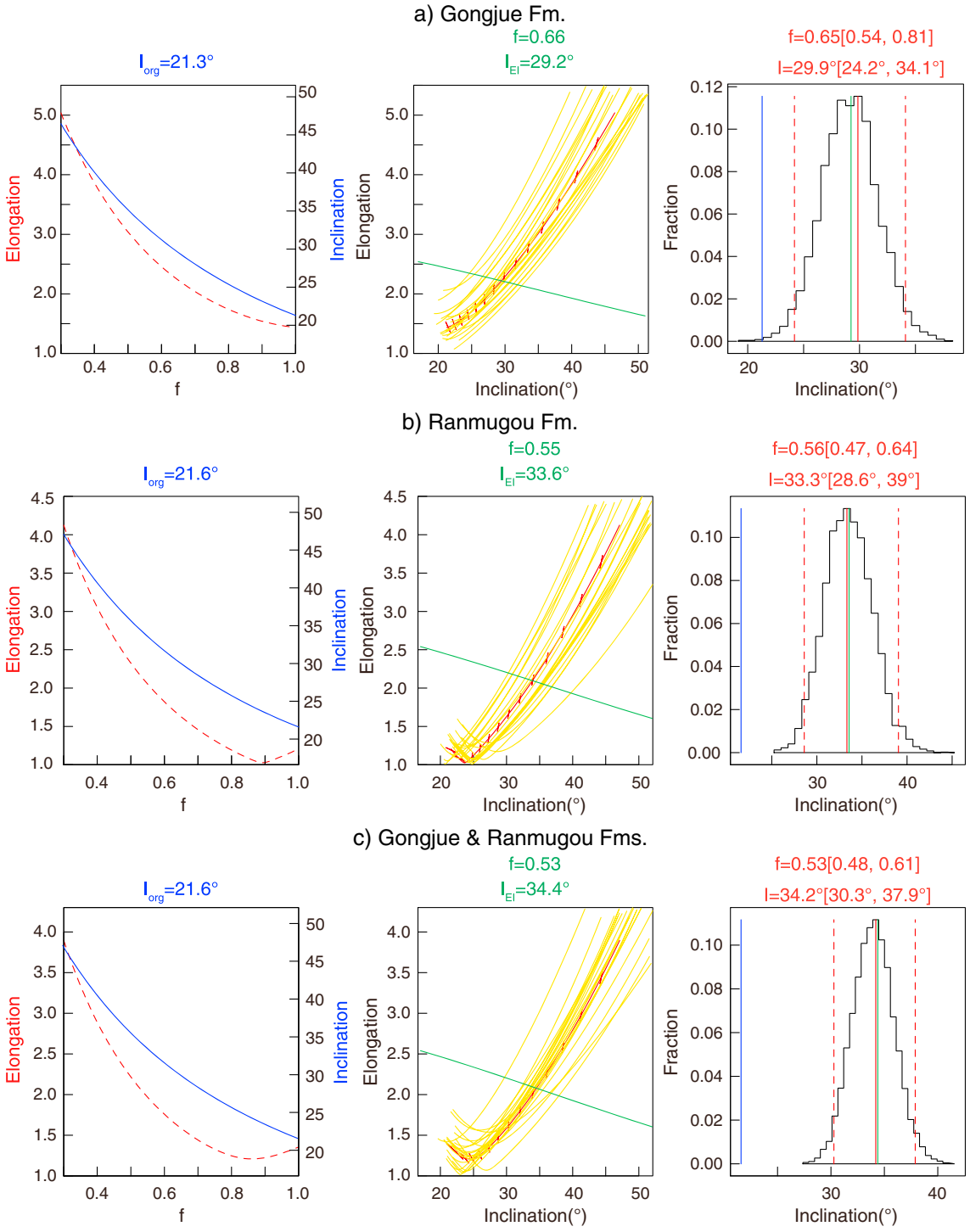

Figure 9. Correction for the inclination error of the ChRMs from the Gongjue formation (a), the Ranmugou formation (b), and the combined two formations (c) using the E/I method (Tauxe & Kent, 2004).

during deposition of the E_{2r}^{2} and E_{2r}^{3} (Torsvik et al., 2012). The window-mean declination at site level 5 is 36.1 ± 3.4°, which means the window-mean declination at this site level was 45.3 ± 3.9° soon after deposition of E_{2r}^{1}. In this manner, a clockwise rotation of 33.3 ± 3.4° during deposition of the E_{2g} and E_{2r}^{1} can be calculated with respect to the Eurasian APWP (Torsvik et al., 2012). The net effect will be that the Gongjue basin has experienced a total clockwise rotation of 24.1 ± 3.1° since the deposition of the red

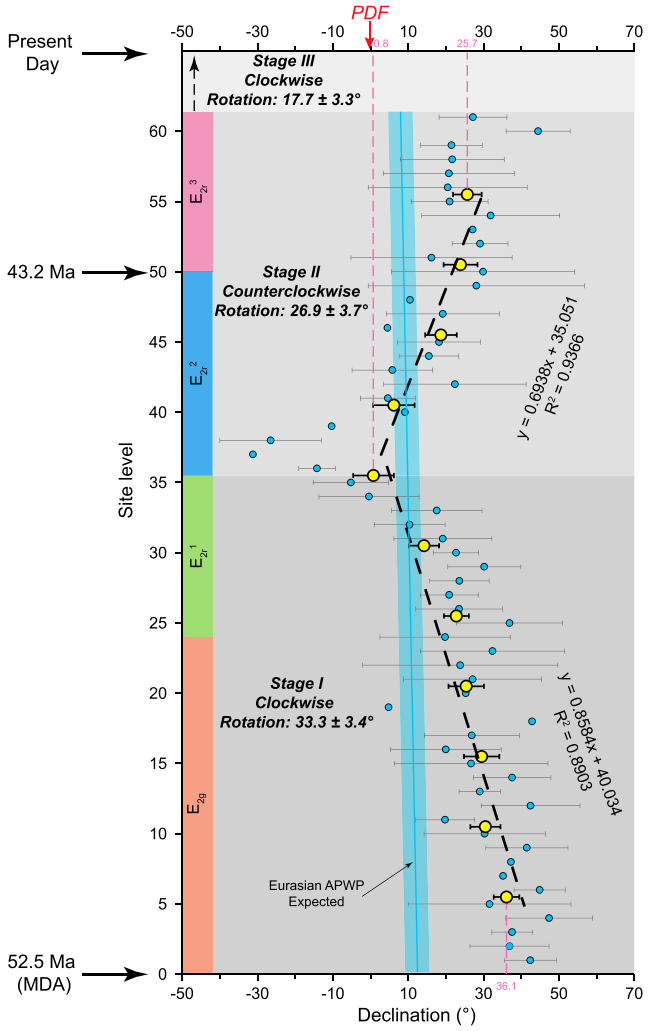

Figure 10. Stratigraphic analyses of the declinations and error bars of site-mean (blue dots) and 10 successive sites sliding window-mean (yellow dots) ChRM directions of the red beds in the Gongjue basin. Sites are plotted according to the site level; the distance of adjacent sites is assigned to be "1." Details of the calculation can be found in the main text and Table S6. MDA, maximum depositional age; PDF, present day geomagnetic field.

beds, of which 6.4 ± 3.6° occurred during the deposition of the red beds and the rest 17.7 ± 3.3° happened after deposition.

Therefore, the Gongjue basin has experienced three stages of rotation relative to the Eurasian APWP since the deposition of the red beds: Stage I clockwise rotation of 33.3 ± 3.4° occurred during deposition of the E_{2g} and E_{2r}^{1}; Stage II counterclockwise rotation of 26.9 ± 3.7° happened during deposition of the E_{2r}^{2} and E_{2r}^{3}; and Stage III clockwise rotation of 17.7 ± 3.3° occurred after deposition of the Gongjue red beds. This complex rotation history can explain why best grouping of the ChRM directions was reached at ~79–91% rather than ~100% as for primary remanence of pre-folding origin. It also probably accounts for the failure of applying E/I method to our data set for inclination shallowing correction. The sampled limited stratigraphic profile of Tong et al. (2017) possibly records insignificant within section rotation, which may explain the success of their E/I correction.

7.3. Regional Implications

No paleomagnetic result has been reported from the Cenozoic rocks in the eastern part of the Lhasa terrane, whereas available paleomagnetic results from the eastern Qiangtang are from the Nangqian, Xialaxiu, Gongjue, and Mangkang basins from west to east. The latest robust paleomagnetic results from volcanic rocks of the Nangqian basin to the northwest of our study area indicate ~10° of clockwise rotation relative to the Eurasian APWP after eruption at 38–37 Ma, whereas volcanic rocks (51–49 Ma) in the Xialaxiu basin, 50 km northeastern of the Nangqian basin, show negligible rotation (Roperch et al., 2017). The paleomagnetic results from the Xialaxiu volcanic rocks contradict the results from the Paleocene-Eocene red beds in the same basin, which indicate ~45° of counterclockwise rotation (Cogné et al., 1999). These red beds in the Xialaxiu basin may, however, have been remagnetized (Roperch et al., 2017). To the east, the Gongjue basin has experienced a cumulative clockwise rotation of 24.1 ± 3.1° relative to the Eurasian APWP as we find in this study. Paleomagnetic results of the Lower and Upper Cretaceous red beds in the Mangkang basin indicate ~42° and ~36° of clockwise rotation relative to the Eurasian APWP (Huang et al., 1992; Otofuji et al., 1990; Tong, Yang, Gao, et al., 2015), respectively. Farther south around the eastern Himalayan syntaxis, rotation values increase to ~70–90° (e.g., Huang et al., 1993; Li et al., 2018; Tanaka et al., 2008). Paleomagnetic results from the Nangqian, Xialaxiu, Gongjue, and Mangkang basins thus indicate that the eastern Qiangtang underwent Cenozoic net clockwise rotation, and the amount of the rotation appears to increase eastward, proportional to strike. This indicates that the Lhasa and Qiangtang terranes were more straight before the India-Asia collision with a less marked arcuation at the eastern plateau margin. This is consistent with and supports previous propositions that the accurate shape of the eastern margin of the Tibetan Plateau results at least partly from dextral shear accommodating the Indian indentation (Chen & Gerya, 2016; Dupont-Nivet et al., 2004; England & Molnar, 1990). However, other processes such as extrusion and/or local shear along strike-slip faults are also consistent with rotations. The timing of the rotations enables to better constrain their potential relationships to regional tectonic processes, in particular in the Gongjue Basin.

First, we note that there is a relatively small time window (≥5 Myr) between the deposition of the Gongjue red beds (maximum depositional age of ca. 53 Ma) and the initiation of the India-Asia collision (~58 Ma; e.g., DeCelles et al., 2014; Hu, Garzanti, et al., 2015; Hu, Wang, et al., 2015; Orme et al., 2014; Spurlin et al., 2005). Possibly, the clockwise rotation started earlier in the eastern Qiangtang. Therefore, we infer that the revealed net clockwise rotations of the eastern Qiangtang terrane from the Gongjue basin are minimum estimates of the rotation after onset of the India-Asia collision. The eastern Qiangtang may have originally been linear, EW

oriented, without arcuation before the onset of the India-Asia collision in line with the Neotethys slab (Van der Voo et al., 1999; van Hinsbergen et al., 2012; Yi et al., 2015). The first two phases of rotation occur within 53 and 43 Ma and therefore can be attributed to the early deformation associated with the collision. It also indicates that the Qiangtang terrane was actively deforming at this time. This is in good agreement with tectonic models depicting deformation and uplift starting from the central Tibetan Plateau followed by plateau growth to the north and south (e.g., Wang et al., 2008).

In detail, the complex suite of rotational events recorded in the Gongjue Basin can be linked to successive tectonic events affecting this area. Recent restoration of the NW Indochina extrusion has indicated ~600 km of left-lateral motion along the NW part of the Ailao Shan-Red River fault, ~350 km of which was accommodated by clockwise rotation, and deformation within NW Indochina which started in Eocene times, and the remaining ~250 km motion was accommodated by extrusion of the entire Indochina along the entire Ailao Shan-Red River fault in Oligocene-Miocene times (Li, Advokaat, et al., 2017). Such a large extrusion value requires that the Lhasa and Qiangtang terranes underwent a Cenozoic counterclockwise rotation of ~20° (Royden et al., 2008), which is consistent with the reported paleomagnetic results from the western and middle parts of the Lhasa and Qiangtang terranes. This regional counterclockwise rotation is a regional effect of extrusion and should have occurred simultaneously with the extrusion of Indochina. The revealed three stages of rotation of the Gongjue Basin may correlate to the extrusion and rotation history of Indochina: Stage I clockwise rotation of the Gongjue basin may correspond to the associated distributed dextral shearing among the shortening Tibetan plateau, the rigid South China, and extruding Indochina blocks. It would reflect the clockwise rotation and deformation of NW Indochina along the NW part of the Ailao Shan Fault at Early Eocene-early middle Eocene times. Stage II counterclockwise rotation may reflect the regional behavior of the Qiangtang terrane induced by extrusion of the Indochina blocks. This stage of rotation was coeval with the extrusion of NW Indochina blocks, implying that extrusion of Indochina along the NW part of the Ailao Shan-Red River fault zone started in middle Eocene time. Stage III local clockwise rotation after middle Eocene could then also be linked to the regional clockwise rotation of the Indochina block associated with its wholesale extrusion along the Ailao Shan-Red River fault by clockwise rotation (Li, Advokaat, et al., 2017). Therefore, Stage I clockwise rotation and Stage II counterclockwise rotation of the Gongjue basin may mark the transition from local internal NW Indochina deformation and rotation along NW Ailao Shan-Red River fault to the regional rotation of the whole Indochina along the entire Ailao Shan-Red River fault.

8. Conclusions

The Gongjue basin, located in the eastern Qiangtang terrane, is mainly filled with red beds divided into the Gongjue formation (E_{2g}) and the Ranmugou formation (E_{2r}) with volcanic rocks (~43 Ma) in the middle part of the Ranmugou formation (E_{2r}^{2}). In this paper, we applied geochronologic and paleomagnetic investigations of the red beds from both formations to constrain the kinematic evolution of eastern Tibet. Our analyses lead us to conclude the following:

1. Detrital zircon U-Pb geochronology has constrained the maximum deposition age of the Gongjue red beds of 52.5 ± 1.5 Ma.
2. The magnetic carriers of the Gongjue red beds are a combination of detrital magnetite and hematite.
3. The ChRM of the Gongjue red beds is depositional remanent magnetization with primary origin.
4. Red beds from the Gongjue formation and Ranmugou formation have a mean ChRM directions of D_s = 31.0°, I_s = 21.3° (n = 150, k = 16.8, α_{95} = 2.9°) and D_s = 15.9°, I_s = 22.0° (n = 178, k = 12.7, α_{95} = 3.1°), respectively, showing that rotation occurred during the deposition of the two formations within 53–43 Ma.
5. The Gongjue basin underwent 24.1 ± 3.1° of clockwise rotation relative to the Eurasian APWP since the deposition of the red beds. Three stages of rotation are recognized: Stage I clockwise rotation of 33.3 ± 3.4° occurred during deposition of E_{2g} and E_{2r}^{1} within 53–43 Ma; Stage II counterclockwise rotation of 26.9 ± 3.7° happened during deposition of E_{2r}^{2} and E_{2r}^{3} within 53–43 Ma; and Stage III clockwise rotation of 17.7 ± 3.3° occurred after deposition of the Gongjue red beds (after 43 Ma).

Acknowledgments
W. H. was supported by the Netherlands Organization for Scientific Research (NWO) with a Rubicon grant (825.15.016). D. J. J. v. H. was funded through NWO VIDI grant 864.11.004. G. D.-N. acknowledges funding from the ANR DSP-Tibet and ERC 649081 (MAGIC) grants. Z. G. was supported by China National Science and Technology Major Project (no. 2017ZX05008001). We are grateful to Yo-ichiro Otofuji, an anonymous reviewer, and the Associate Editor Mark J. Dekkers for their constructive comments and suggestions.

References

Bureau of Geology and Mineral Resources of Xizang Autonomous Region (1993). *Regional geology of Xizang (Tibet) Autonomous Region*, *Geological Memoirs Series* (Vol. 1, Number 31, p. 707). Beijing: Geological House.

Chen, J., Huang, B., & Sun, L. (2010). New constraints to the onset of the India-Asia collision: Paleomagnetic reconnaissance on the Linzizong Group in the Lhasa Block, China. *Tectonophysics*, *489*(1–4), 189–209. https://doi.org/10.1016/j.tecto.2010.04.024

Chen, J., Huang, B., Yi, Z., Yang, L., & Chen, L. (2014). Paleomagnetic and $^{40}Ar/^{39}Ar$ geochronological results from the Linzizong Group, Linzhou Basin, Lhasa Terrane, Tibet: Implications to Paleogene paleolatitude and onset of the India-Asia collision. *Journal of Asian Earth Sciences*, *96*, 162–177. https://doi.org/10.1016/j.jseaes.2014.09.007

Chen, L., & Gerya, T. V. (2016). The role of lateral lithospheric strength heterogeneities in orogenic plateau growth: Insights from 3-D thermo-mechanical modeling. *Journal of Geophysical Research: Solid Earth*, *121*, 3118–3138. https://doi.org/10.1002/2016JB012872

Chen, Y., Cogne, J. P., Courtillot, V., Tapponnier, P., & Zhu, X. Y. (1993). Cretaceous paleomagnetic results from western Tibet and tectonic implications. *Journal of Geophysical Research*, *98*(B10), 17,981–17,999. https://doi.org/10.11029/17993JB01006

Cheng, F., Jolivet, M., Dupont-Nivet, G., Wang, L., Yu, X., & Guo, Z. (2015). Lateral extrusion along the Altyn Tagh Fault, Qilian Shan (NE Tibet): Insight from a 3D crustal budget. *Terra Nova*, *27*(6), 416–425. https://doi.org/10.1111/ter.12173

Cogné, J. P., Halim, N., Chen, Y., & Courtillot, V. (1999). Resolving the problem of shallow magnetizations of Tertiary age in Asia: Insights from paleomagnetic data from the Qiangtang, Kunlun, and Qaidam blocks (Tibet, China), and a new hypothesis. *Journal of Geophysical Research*, *104*(B8), 17,715–17,734. https://doi.org/10.11029/11999JB900153

Cook, K. L., & Royden, L. H. (2008). The role of crustal strength variations in shaping orogenic plateaus, with application to Tibet. *Journal of Geophysical Research*, *113*, B08407. https://doi.org/10.01029/02007JB005457

Copley, A., Avouac, J. P., & Royer, J. Y. (2010). The India-Asia collision and the Cenozoic slowdown of the Indian plate: Implications for the forces driving plate motions. *Journal of Geophysical Research*, *115*, B03410. https://doi.org/10.01029/02009JB006634

DeCelles, P., Kapp, P., Gehrels, G., & Ding, L. (2014). Paleocene-Eocene foreland basin evolution in the Himalaya of southern Tibet and Nepal: Implications for the age of initial India-Asia collision. *Tectonics*, *33*, 824–849. https://doi.org/10.1002/2014TC003522

Ding, J., Zhang, S., Chen, W., Zhang, J., Yang, T., Jiang, G., et al. (2015). Paleomagnetism of the Oligocene Kangtuo Formation red beds (Central Tibet): Inclination shallowing and tectonic implications. *Journal of Asian Earth Sciences*, *104*, 55–68. https://doi.org/10.1016/j.jseaes.2014.10.006

Dunlop, D. J., & Ödemir, Ö. (1997). *Rock magnetism: Fundamentals and frontiers* (p. 573). Cambridge: Cambridge University Press.

Dupont-Nivet, G., Guo, Z., Butler, R. F., & Jia, C. (2002). Discordant paleomagnetic direction in Miocene rocks from the central Tarim Basin: Evidence for local deformation and inclination shallowing. *Earth and Planetary Science Letters*, *199*(3–4), 473–482. https://doi.org/10.1016/S0012-821X(02)00566-6

Dupont-Nivet, G., Horton, B. K., Butler, R. F., Wang, J., Zhou, J., & Waanders, G. L. (2004). Paleogene clockwise tectonic rotation of the Xining-Lanzhou region, northeastern Tibetan Plateau. *Journal of Geophysical Research*, *109*, B04401. https://doi.org/10.1029/2003JB002620

Dupont-Nivet, G., Lippert, P. C., van Hinsbergen, D. J. J., Meijers, M. J. M., & Kapp, P. (2010). Palaeolatitude and age of the Indo-Asia collision: Palaeomagnetic constraints. *Geophysical Journal International*, *182*(3), 1189–1198. https://doi.org/10.1111/j.1365-246X.2010.04697.x

Dupont-Nivet, G., van Hinsbergen, D. J. J., & Torsvik, T. H. (2010). Persistently low Asian paleolatitudes: Implications for the India-Asia collision history. *Tectonics*, *29*, TC5016. https://doi.org/10.1029/2008TC002437

Egli, R. (2004). Characterization of individual rock magnetic components by analysis of remanence curves, 1. Unmixing natural sediments. *Studia Geophysica et Geodaetica*, *48*(2), 391–446.

England, P., & Molnar, P. (1990). Right-lateral shear and rotation as the explanation for strike-slip faulting in eastern Tibet. *Nature*, *344*(6262), 140–142. https://doi.org/10.1038/344140a0

Fisher, R. A. (1953). Dispersion on a sphere. *Proceedings of the Royal Society of London. Series A: Mathematical and Physical Sciences*, *217*(1130), 295–305. https://doi.org/10.1098/rspa.1953.0064

Gilder, S., Chen, Y., Cogne, J.-P., Tan, X., Courtillot, V., Sun, D., & Li, Y. (2003). Paleomagnetism of Upper Jurassic to Lower Cretaceous volcanic and sedimentary rocks from the western Tarim Basin and implications for inclination shallowing and absolute dating of the M-0 (ISEA?) chron. *Earth and Planetary Science Letters*, *206*(3–4), 587–600. https://doi.org/10.1016/S0012-821X(02)01074-9

Heslop, D., McIntosh, G., & Dekkers, M. (2004). Using time-and temperature-dependent Preisach models to investigate the limitations of modelling isothermal remanent magnetization acquisition curves with cumulative log Gaussian functions. *Geophysical Journal International*, *157*(1), 55–63.

Horton, B. K., Yin, A., Spurlin, M. S., Zhou, J., & Wang, J. (2002). Paleocene-Eocene syncontractional sedimentation in narrow, lacustrine-dominated basins of east-central Tibet. *Geological Society of America Bulletin*, *114*(7), 771–786.

Hrouda, F. S. (1991). Models of magnetic anisotropy variations in sedimentary thrust sheets. *Tectonophysics*, *185*(3–4), 203–210. https://doi.org/10.1016/0040-1951(91)90444-W

Hu, X., Garzanti, E., Moore, T., & Raffi, I. (2015). Direct stratigraphic dating of India-Asia collision onset at the Selandian (middle Paleocene, 59 ± 1 Ma). *Geology*, *43*(10), 859–862.

Hu, X., Wang, J., BouDagher-Fadel, M., Garzanti, E., & An, W. (2015). *New insights into the timing of the India–Asia collision from the Paleogene Quxia and Jialazi formations of the Xigaze forearc basin*. South Tibet: Gondwana Research.

Huang, H., Peng, Z., Lu, W., & Zheng, J. (1993). Paleomagnetic division and comparison of the Tertiary system in Jiuxi and Jiudong basins (in Chinese). *Gansu Geology*, *1993*, 6–16.

Huang, K., & Opdyke, N. D. (2015). Post-folding magnetization of the Triassic rocks from western Guizhou and southern Yunnan provinces: New evidence for large clockwise rotations in the Simao terrane. *Earth and Planetary Science Letters*, *423*, 155–163. https://doi.org/10.1016/j.epsl.2015.05.015

Huang, K., Opdyke, N. D., Li, J., & Peng, X. (1992). Paleomagnetism of Cretaceous rocks from eastern Qiangtang terrane of Tibet. *Journal of Geophysical Research*, *97*(B2), 1789–1799. https://doi.org/10.1029/1791JB02747

Huang, W., Dupont-Nivet, G., Lippert, P. C., van Hinsbergen, D. J. J., Dekkers, M. J., Waldrip, R., et al. (2015). What was the Paleogene latitude of the Lhasa terrane? A reassessment of the geochronology and paleomagnetism of Linzizong volcanic rocks (Linzhou Basin, Tibet). *Tectonics*, *34*, 594–622. https://doi.org/10.1002/2014TC003787

Huang, W., Dupont-Nivet, G., Lippert, P. C., van Hinsbergen, D. J. J., & Hallot, E. (2013). Inclination shallowing in Eocene Linzizong sedimentary rocks from southern Tibet: Correction, possible causes and implications for reconstructing the India–Asia collision. *Geophysical Journal International*, *194*(3), 1390–1411. https://doi.org/10.1093/gji/ggt188

Huang, W., van Hinsbergen, D. J. J., Maffione, M., Orme, D. A., Dupont-Nivet, G., Guilmette, C., et al. (2015). Lower Cretaceous Xigaze ophiolite formed in the Gangdese forearc: Evidence from paleomagnetism, sediment provenance, and stratigraphy. *Earth and Planetary Science Letters*, *415*, 142–153. https://doi.org/10.1016/j.epsl.2015.01.032

Huang, W., Dupont-Nivet, G., Lippert, P., Van Hinsbergen, D. J. J., Dekkers, M., Guo, Z., et al. (2015). Can a primary remanence be retrieved from partially remagnetized Eocence volcanic rocks in the Nanmulin Basin (southern Tibet) to date the India-Asia collision? *Journal of Geophysical Research - Solid Earth*, *120*, 42–66. https://doi.org/10.1002/2014JB011599

Jackson, M. J., Banerjee, J. A., Marvin, R. L., & Grueber, W. (1991). Detrital remanence inclination errors, and anhysteretic remanence anisotropy: Quantitative model and experimental results. *Geophysical Journal International*, *104*(1), 95–103. https://doi.org/10.1111/j.1365-246X.1991.tb02496.x

Jelinek, V. (1981). Characterization of the magnetic fabric of rocks. *Tectonophysics*, *79*(3-4), T63–T67. https://doi.org/10.1016/0040-1951(81)90110-4

Jezek, J., & Gilder, S. A. (2006). Competition of magnetic and hydrodynamic forces on ellipsoidal particles under shear: Influence of the Earth's magnetic field on particle alignment in viscous media. *Journal of Geophysical Research*, *111*, B12S23. https://doi.org/10.1029/2006JB004541

Johnson, M. R. W. (2002). Shortening budgets and the role of continental subduction during the India-Asia collision. *Earth-Science Reviews*, *59*(1–4), 101–123. https://doi.org/10.1016/S0012-8252(02)00071-5

Kapp, P., DeCelles, P. G., Gehrels, G. E., Heizler, M., & Ding, L. (2007). Geological records of the Lhasa-Qiangtang and Indo-Asian collisions in the Nima area of central Tibet. *Geological Society of America Bulletin*, *119*(7–8), 917–933. https://doi.org/10.1130/B26033.1

Kapp, P., Yin, A., Harrison, T. M., & Ding, L. (2005). Cretaceous-Tertiary shortening, basin development, and volcanism in Central Tibet. *Geological Society of America Bulletin*, *117*(7), 865–878. https://doi.org/10.1130/B25595.1

King, R. F. (1955). The remanent magnetism of artificially deposited sediments. *Geophysical Journal International*, *7*, 115–134. https://doi.org/10.1111/j.1365-246X.1955.tb06558.x

Kirschvink, J. (1980). The least-squares line and plane and the analysis of palaeomagnetic data. *Geophysical Journal International*, *62*(3), 699–718. https://doi.org/10.1111/j.1365-246X.1980.tb02601.x

Kodama, K. P. (2009). Simplification of the anisotropy-based inclination correction technique for magnetite- and haematite-bearing rocks: A case study for the Carboniferous Glenshaw and Mauch Chunk Formations, North America. *Geophysical Journal International*, *176*(2), 467–477. https://doi.org/10.1111/j.1365-246X.2008.04013.x

Koymans, M. R., Langereis, C. G., Pastor-Galán, D., & van Hinsbergen, D. J. (2016). Paleomagnetism.org: An online multi-platform open source environment for paleomagnetic data analysis. *Computers & Geosciences*, *93*, 127–137. https://doi.org/10.1016/j.cageo.2016.05.007

Kruiver, P. P., Dekkers, M. J., & Heslop, D. (2001). Quantification of magnetic coercivity components by the analysis of acquisition curves of isothermal remanent magnetisation. *Earth and Planetary Science Letters*, *189*(3-4), 269–276. https://doi.org/10.1016/S0012-821X(01)00367-3

Kruiver, P. P., & Passier, H. F. (2001). Coercivity analysis of magnetic phases in sapropel S1 related to variations in redox conditions, including an investigation of the S-ratio. *Geochemistry, Geophysics, Geosystems*, *2*(12). https://doi.org/10.1029/2001GC000181

Li, S., Advokaat, E. L., van Hinsbergen, D. J., Koymans, M., Deng, C., & Zhu, R. (2017). Paleomagnetic constraints on the Mesozoic-Cenozoic paleolatitudinal and rotational history of Indochina and South China: Review and updated kinematic reconstruction. *Earth-Science Reviews*, *171*, 58–77. https://doi.org/10.1016/j.earscirev.2017.05.007

Li, S., Hinsbergen, D. J., Deng, C., Advokaat, E. L., & Zhu, R. (2018). Paleomagnetic constraints from the baoshan area on the deformation of the Qiangtang-Sibumasu terrane around the eastern Himalayan syntaxis. *Journal of Geophysical Research - Solid Earth*, *123*, 977–997. https://doi.org/10.1002/2017JB015112

Li, S., Yang, Z., Deng, C., He, H., Qin, H., Sun, L., et al. (2017). Clockwise rotations recorded in redbeds from the Jinggu Basin of northwestern Indochina. *Geological Society of America Bulletin*, *129*(9–10), 1100–1122. https://doi.org/10.1130/B31637.1

Lippert, P. C., Zhao, X. X., Coe, R. S., & Lo, C. H. (2011). Palaeomagnetism and $^{40}Ar/^{39}Ar$ geochronology of upper Palaeogene volcanic rocks from Central Tibet: Implications for the Central Asia inclination anomaly, the palaeolatitude of Tibet and post-50 Ma shortening within Asia. *Geophysical Journal International*, *184*(1), 131–161. https://doi.org/10.1111/j.1365-246X.2010.04833.x

Løvlie, R., & Torsvik, T. (1984). Magnetic remanence and fabric properties of laboratory-deposited hematite-bearing red sandstone. *Geophysical Research Letters*, *11*(3), 221–224. https://doi.org/10.1029/GL1011i1003p00221

Ma, Y., Yang, T., Bian, W., Jin, J., Wang, Q., Zhang, S., et al. (2017). Paleomagnetic and geochronologic results of latest Cretaceous lava flows from the Lhasa terrane and their tectonic implications. *Journal of Geophysical Research: Solid Earth*, *122*, 8786–8809. https://doi.org/10.1002/2017JB014743

Ma, Y., Yang, T., Yang, Z., Zhang, S., Wu, H., Li, H., et al. (2014). Paleomagnetism and U-Pb zircon geochronology of Lower Cretaceous lava flows from the western Lhasa terrane: New constraints on the India–Asia collision process and intracontinental deformation within Asia. *Journal of Geophysical Research: Solid Earth*, *119*, 7404–7424. https://doi.org/10.1002/2014JB011362

Metcalfe, I. (2013). Gondwana dispersion and Asian accretion: Tectonic and palaeogeographic evolution of eastern Tethys. *Journal of Asian Earth Sciences*, *66*, 1–33. https://doi.org/10.1016/j.jseaes.2012.12.020

Orme, D. A., Carrapa, B., & Kapp, P. (2014). Sedimentology, provenance and geochronology of the Upper Cretaceous–lower Eocene western Xigaze forearc basin, southern Tibet. *Basin Research*, 1–25. https://doi.org/10.1111/bre.12080,%20doi:10.1111/bre.12080

Otofuji, Y., Inoue, S., Funahara, S., Murata, F., & Zheng, X. (1990). Palaeomagnetic study of eastern Tibet-deformation of the three rivers region. *Geophysical Journal International*, *103*(1), 85–94. https://doi.org/10.1111/j.1365-246X.1990.tb01754.x

Pubellier, M., Chamot-Rooke, N., Ego, F., Guezou, J., Konstantinovskaya, E., Rabaute, A., & Ringenbach, J. (2008). *Structural map of eastern Eurasia*. Paris: Commission for the Geological Map of the World, scale.

Pusok, A., & Kaus, B. J. (2015). Development of topography in 3-D continental-collision models. *Geochemistry, Geophysics, Geosystems*, *16*, 1378–1400. https://doi.org/10.1002/2015GC005732

Replumaz, A., & Tapponnier, P. (2003). Reconstruction of the deformed collision zone between India and Asia by backward motion of lithospheric blocks. *Journal of Geophysical Research*, *108*(B6), 2285. https://doi.org/10.1029/2001JB000661

Roberts, A. P., Cui, Y., & Verosub, K. L. (1995). Wasp-waisted hysteresis loops: Mineral magnetic characteristics and discrimination of components in mixed magnetic systems. *Journal of Geophysical Research*, *100*(B9), 17,909–17,924. https://doi.org/10.11029/17995JB00672

Roperch, P., Dupont-Nivet, G., Guillot, S., Goussin, F., Huang, W., Replumaz, A., et al. (2017). Paleomagnetic constraints on early collisional deformation along the eastern margin of the Qiangtang terrane (Tibetan plateau) at 50 and 37 Ma, paper presented at EGU General Assembly Conference Abstracts.

Royden, L. H., Burchfiel, B. C., & van der Hilst, R. D. (2008). The geological evolution of the Tibetan Plateau. *Science*, *321*(5892), 1054–1058. https://doi.org/10.1126/science.1155371

Sensor, A. M. C., & Natalin, B. A. (1996). Paleotectonic of Asia: Fragment of a synthesis. In A. N. Yin & T. M. Harrison (Eds.), *The tectonic evolution of Asia* (pp. 486–640). Cambridge: Cambridge University Press.

Spurlin, M. S., Yin, A., Horton, B. K., Zhou, J., & Wang, J. (2005). Structural evolution of the Yushu-Nangqian region and its relationship to syncollisional igneous activity, east-central Tibet. *Geological Society of America Bulletin*, *117*, 1293–1317. https://doi.org/10.1130/B25572.25571

Studnicki-Gizbert, C., Burchfiel, B., Li, Z., & Chen, Z. (2008). Early Tertiary Gonjo basin, eastern Tibet: Sedimentary and structural record of the early history of India-Asia collision. *Geosphere*, *4*(4), 713–735. https://doi.org/10.1130/GES00136.1

Tan, X., Gilder, S., Kodama, K. P., Jiang, W., Han, Y., Zhang, H., et al. (2010). New paleomagnetic results from the Lhasa block: Revised estimation of latitudinal shortening across Tibet and implications for dating the India-Asia collision. *Earth and Planetary Science Letters*, *293*(3-4), 396–404. https://doi.org/10.1016/j.epsl.2010.03.013

Tanaka, K., Mu, C., Sato, K., Takemoto, K., Miura, D., Liu, Y., et al. (2008). Tectonic deformation around the eastern Himalayan syntaxis: Constraints from the Cretaceous palaeomagnetic data of the Shan-Thai Block. *Geophysical Journal International*, *175*(2), 713–728. https://doi.org/10.1111/j.1365-246X.2008.03885.x

Tang, M., Liu-Zeng, J., Hoke, G. D., Xu, Q., Wang, W., Li, Z., et al. (2017). Paleoelevation reconstruction of the Paleocene-Eocene Gonjo basin, SE-central Tibet. *Tectonophysics*, *712*, 170–181.

Tapponnier, P., Peltzer, G., Le Dain, A. Y., Armijo, R., & Cobbold, P. (1982). Propagating extrusion tectonics in Asia: New insights from simple experiments with plasticine. *Geology*, *10*(12), 611–616. https://doi.org/10.1130/0091-7613(1982)10%3C611:PETIAN%3E2.0.CO;2

Tauxe, L. (2010). *Essentials of paleomagnetism*. Oakland, CA: University of California Press.

Tauxe, L., & Kent, D. V. (2004). A simplified statistical model for the geomagnetic field and the detection of shallow bias in paleomagnetic inclinations: Was the ancient magnetic field dipolar? In J. E. T. Channell, et al. (Eds.), *Timescales of the paleomagnetic field, Geophysical Monograph Series* (Vol. 145, pp. 101–116). https://doi.org/10.1029/145GM08

Tauxe, L., Mullender, T., & Pick, T. (1996). Potbellies, wasp-waists, and superparamagnetism in magnetic hysteresis. *Journal of Geophysical Research*, *101*(B1), 571–583. https://doi.org/10.1029/1095JB03041

Tauxe, L., & Watson, G. (1994). The fold test: An eigen analysis approach. *Earth and Planetary Science Letters*, *122*(3-4), 331–341. https://doi.org/10.1016/0012-821X(94)90006-X

Tong, Y., Yang, Z., Jing, X., Zhao, Y., Li, C., Huang, D., & Zhang, X. (2016). New insights into the Cenozoic lateral extrusion of crustal blocks on the southeastern edge of Tibetan Plateau: Evidence from paleomagnetic results from Paleogene sedimentary strata of the Baoshan terrane. *Tectonics*, *35*, 2494–2514. https://doi.org/10.1002/2016TC004221

Tong, Y., Yang, Z., Mao, C., Pei, J., Pu, Z., & Xu, Y. (2017). Paleomagnetism of Eocene red-beds in the eastern part of the Qiangtang terrane and its implications for uplift and southward crustal extrusion in the southeastern edge of the Tibetan Plateau. *Earth and Planetary Science Letters*, *475*, 1–14. https://doi.org/10.1016/j.epsl.2017.07.026

Tong, Y.-B., Yang, Z., Gao, L., Wang, H., Zhang, X.-D., An, C.-Z., et al. (2015). Paleomagnetism of Upper Cretaceous red-beds from the eastern Qiangtang block: Clockwise rotations and latitudinal translation during the India–Asia collision. *Journal of Asian Earth Sciences*, *114*, 732–749. https://doi.org/10.1016/j.jseaes.2015.08.016

Tong, Y.-B., Yang, Z., Wang, H., Gao, L., An, C.-Z., Zhang, X.-D., & Xu, Y.-C. (2015). The Cenozoic rotational extrusion of the Chuan Dian fragment: New paleomagnetic results from Paleogene red-beds on the southeastern edge of the Tibetan plateau. *Tectonophysics*, *658*, 46–60. https://doi.org/10.1016/j.tecto.2015.07.007

Torsvik, T. H., Van der Voo, R., Preeden, U., Mac Niocaill, C., Steinberger, B., Doubrovine, P. V., et al. (2012). Phanerozoic polar wander, palaeogeography and dynamics. *Earth-Science Reviews*, *114*(3-4), 325–368. https://doi.org/10.1016/j.earscirev.2012.06.007

Turner, M. B., Cronin, S. J., Stewart, R. B., Bebbington, M., & Smith, I. E. (2008). Using titanomagnetite textures to elucidate volcanic eruption histories. *Geology*, *36*(1), 31–34. https://doi.org/10.1130/G24186A.1

Van der Voo, R., Spakman, W., & Bijwaard, H. (1999). Tethyan subducted slabs under India. *Earth and Planetary Science Letters*, *171*, 7–20.

van Hinsbergen, D. J., Steinberger, B., Doubrovine, P. V., & Gassmöller, R. (2011). Acceleration and deceleration of India-Asia convergence since the Cretaceous: Roles of mantle plumes and continental collision. *Journal of Geophysical Research*, *116*, B06101. https://doi.org/10.1029/2010JB008051

van Hinsbergen, D. J. J., Kapp, P., Dupont-Nivet, G., Lippert, P. C., Decelles, P. G., & Torsvik, T. H. (2011). Restoration of Cenozoic deformation in Asia and the size of Greater India. *Tectonics*, *30*, TC5003. https://doi.org/10.1029/2011TC002908

van Hinsbergen, D. J. J., Lippert, P. C., Dupont-Nivet, G., McQuarrie, N., Doubrovine, P. V., Spakman, W., & Torsvik, T. H. (2012). Greater India Basin hypothesis and a two-stage Cenozoic collision between India and Asia. *Proceedings of the National Academy of Sciences*, *109*(20), 7659–7664. https://doi.org/10.1073/pnas.1117262109

Wang, C., Zhao, X., Liu, Z., Lippert, P. C., Graham, S. A., Coe, R. S., et al. (2008). Constraints on the early uplift history of the Tibetan Plateau. *Proceedings of the National Academy of Sciences*, *105*(13), 4987–4992. https://doi.org/10.1073/pnas.0703595105

Yan, M., Van der Voo, R., Tauxe, L., Fang, X., & Parés, J. M. (2005). Shallow bias in Neogene palaeomagnetic directions from the Guide Basin, NE Tibet, caused by inclination error. *Geophysical Journal International*, *163*(3), 944–948. https://doi.org/10.1111/j.1365-246X.2005.02802.x

Yan, Y., Huang, B., Zhao, J., Zhang, D., Liu, X., Charusiri, P., & Veeravinantanakul, A. (2017). Large southward motion and clockwise rotation of Indochina throughout the Mesozoic: Paleomagnetic and detrital zircon U–Pb geochronological constraints. *Earth and Planetary Science Letters*, *459*, 264–278. https://doi.org/10.1016/j.epsl.2016.11.035

Yang, T., Ma, Y., Zhang, S., Bian, W., Yang, Z., Wu, H., et al. (2015). New insights into the India-Asia collision process from Cretaceous paleomagnetic and geochronologic results in the Lhasa terrane. *Gondwana Research*, *28*(2), 625–641. https://doi.org/10.1016/j.gr.2014.06.010

Yang, T. N., Hou, Z. Q., Wang, Y., Zhang, H. R., & Wang, Z. L. (2012). Late Paleozoic to Early Mesozoic tectonic evolution of northeast Tibet: Evidence from the Triassic composite western Jinsha-Garzê-Litang suture. *Tectonics*, *31*, TC4004. https://doi.org/10.1029/2011TC003044

Yang, Z., & Besse, J. (1993). Paleomagnetic study of Permian and Mesozoic sedimentary rocks from northern Thailand support the extrusion model for Indochina. *Earth and Planetary Science Letters*, *117*, 507–524.

Yi, Z., Huang, B., Chen, J., Chen, L., & Wang, H. (2011). Paleomagnetism of early Paleogene marine sediments in southern Tibet, China: Implications to onset of the India-Asia collision and size of Greater India. *Earth and Planetary Science Letters*, *309*(1), 153–165.

Yi, Z., Huang, B., Yang, L., Tang, X., Yan, Y., Qiao, Q., et al. (2015). A quasi-linear structure of the southern margin of Eurasia prior to the India-Asia collision: First paleomagnetic constraints from Upper Cretaceous volcanic rocks near the western syntaxis of Tibet. *Tectonics*, *34*, 1431–1451. https://doi.org/10.1002/2014TC003571

Yin, A., & Harrison, M. T. (2000). Geologic evolution of the Himalayan-Tibetan orogen. *Annual Review of Earth and Planetary Sciences*, *28*(1), 211–280. https://doi.org/10.1146/annurev.earth.28.1.211

Zhao, J., Huang, B., Yan, Y., & Zhang, D. (2015). Late Triassic paleomagnetic result from the Baoshan terrane, West Yunnan of China: Implication for orientation of the east Paleotethys suture zone and timing of the Sibumasu-Indochina collision. *Journal of Asian Earth Sciences*, *111*, 350–364. https://doi.org/10.1016/j.jseaes.2015.06.033

Zhu, D. C., Zhao, Z. D., Niu, Y., Mo, X. X., Chung, S. L., Hou, Z. Q., et al. (2011). The Lhasa terrane: Record of a microcontinent and its histories of drift and growth. *Earth and Planetary Science Letters*, *301*(1-2), 241–255. https://doi.org/10.1016/j.epsl.2010.11.005

Zijderveld, J. D. A. (1967). A.C. demagnetisation of rocks: Analysis of results. In K. M. Creer, D. W. Collinson, & S. K. Runcorn (Eds.), *Methods in palaeomagnetism* (pp. 254–286). Amsterdam: Elsevier.